A subfunctionalization epistasis model to evaluate homeologous gene interactions in allopolyploid wheat

Nicholas Santantonio, Jean-Luc Jannink, Mark E. Sorrells

Cornell University

College of Agriculture and Life Sciences

School of Integrated Plant Science

Plant Breeding and Genetics

December 3, 2018

1   Abstract

Hybridization between related species results in the formation of an allopolyploid with multiple subgenomes. These subgenomes will each contain complete, yet evolutionarily divergent, sets of genes. Like a diploid hybrid, allopolyploids will have two versions, or homeoalleles, for every gene. Partial functional redundancy between homeologous genes should result in a deviation from additivity. These epistatic interactions between homeoalleles are analogous to dominance effects, but are fixed across subgenomes through self pollination. An allopolyploid can be viewed as an immortalized hybrid, with the opportunity to select and fix favorable homeoallelic interactions within inbred varieties. We present a subfunctionalization epistasis model to estimate the degree of functional redundancy between homeoallelic loci and a statistical framework to determine their importance within a population. We provide an

1

example using the homeologous dwarfing genes of allohexaploid wheat, *Rht-1*, and search for genome-wide patterns indicative of homeoallelic subfunctionalization in a breeding population. Using the IWGSC RefSeq v1.0 sequence, 23,796 homeoallelic gene sets were identified and anchored to the nearest DNA marker to form 10,172 homeologous marker sets. Interaction predictors constructed from products of marker scores were used to fit the homeologous main and interaction effects, as well as estimate whole genome genetic values. Some traits displayed a pattern indicative of homeoallelic subfunctionalization, while other traits showed a less clear pattern or were not affected. Using genomic prediction accuracy to evaluate importance of marker interactions, we show that homeologous interactions explain a portion of the non-additive genetic signal, but are less important than other epistatic interactions.

1.1 Keywords

Allopolyploidy | Homeologous | Epistasis | Subfunctionalization | Heterosis | Genomic Prediction

2 Introduction

Whole genome duplication events are ubiquitous in the plant kingdom. The impact of these duplications on angiosperm evolution was not truly appreciated until the ability to sequence entire genomes elucidated their omnipresence (Soltis *et al.*, 2009). Haldane (1933), postulated that single gene duplication allowed one copy to diverge through mutation while metabolic function was maintained by the other copy. Ohno (1970) reintroduced this hypothesis, and it has since been validated both theoretically (Ohta, 1987; Walsh, 1995; Lynch and Conery, 2000), and empirically (Blanc and Wolfe, 2004; Duarte *et al.*, 2005; Liu *et al.*, 2011; Assis and Bachtrog, 2013). The duplicated gene hypothesis does not, however, generally explain the apparent advantage of duplicating an entire suite of genes. The necessity of genetic diversity for plant populations to survive and adapt to divergent or changing environments may help

2

40 to explain this pervasive phenomenon.

41 The need for gene diversity can become more immediate in plants than in animals, where

42 the latter can simply migrate to "greener pastures" when conditions become unfavorable.

43 Plants lack substantial within generation mobility and must therefore change gene expression

44 to cope with changing environmental conditions. Many species maintain gene diversity

45 through alternate splicing, but this has been shown to be less common in plants than in

46 other eukaryotes (Nagasaki *et al.*, 2005). Whole genome duplication can generate the raw

47 materials for the maintenance of genetic diversity (Wendel, 2000; Adams and Wendel, 2005).

48 Gault *et al.* (2018) demonstrated that similar sets of duplicated genes were preserved in two

49 related genera, *Zea* and *Tripsacum*, millions of years after a shared paleopolyploidization

50 event. This conserved pattern in purifying selection suggests that, at least for some genes,

51 there is a clear advantage to maintaining two copies.

52 The union of two complete, yet divergent, genomes during the formation of an allopoly-

53 ploid introduces manifold novel gene pathways that can specialize to specific tissues or en-

54 vironments (Blanc and Wolfe, 2004). Similar to diploid hybrids, the formation of an al-

55 lopolyploid results in a homogeneous population, but heterozygosity is maintained across

56 homeologous sites rather than homologous sites. Unlike diploid hybrids that lose heterozy-

57 gosity in subsequent generations, the homeoallelic heterozygosity is fixed through selfing in

58 the allopolyploid. Mac Key (1970) postulated a trade off between new-creating (allogamous)

59 and self preserving (autogamous) mating systems, where allopolyploids favor self pollination

60 to preserve diverse sets of alleles across their subgenomes. As such, an allopolyploid may be

61 thought of as an immortalized hybrid, with heterosis fixed across subgenomes (Ellstrand and

62 Schierenbeck, 2000; Feldman *et al.*, 2012). While still hotly debated, evidence is mounting

63 that allopolyploids exhibit a true heterotic response as traditional hybrids have demonstrated

64 (Wendel, 2000; Adams and Wendel, 2005; Chen, 2010, 2013).

65 Birchler *et al.* (2010) note that newly synthesized allopolyploids often outperform their

66 sub-genome progenitors, and that the heterotic response appears to be exaggerated in wider

3

67 inter-specific crosses. This seems to hold true even within species, where autopolyploids

68 tend to exhibit higher vigor from wider crosses (Bingham *et al.*, 1994; Segovia-Lerma *et al.*,

69 2004). The overwhelming prevalence of allopolyploidy to autopolyploidy in plant species

70 (Soltis and Soltis, 2009) may suggest that it is the increase in allelic diversity *per se* that

71 is the primary driver for this observed tendency toward genome duplication. Instead of

72 allowing genes to change function after a duplication event, alleles may develop novel function

73 prior to their reunion during an allopolyploidization event. The branched gene networks of

74 the allopoloyploid may provide the organism with the versatility to thrive in a broader

75 ecological landscape than those of its sub-genome ancestors (Mac Key, 1970; Ellstrand and

76 Schierenbeck, 2000; Osborn *et al.*, 2003).

77 Subfunctionalization and neofunctionalization are often described as distinct evolutionary

78 processes. Neofunctionalization implies the duplicated genes have completely novel, non-

79 redundant function (Ohno, 1970). Subfunctionalization is described as a partitioning of

80 ancestral function through degenerative mutations in both copies, such that both genes

81 must be expressed for physiological function (Stoltzfus, 1999; Force *et al.*, 1999; Lynch and

82 Force, 2000). However, barring total functional gene loss, many mutations will have some

83 quantitative effect on protein kinetics or expression (Zeng and Cockerham, 1993). Duplicated

84 genes will demonstrate some quantitative degree of functional redundancy until the ultimate

85 fate of neofunctionalization (i.e. complete additivity) or gene loss (pseudogenization) of one

86 copy. It has been proposed that essentially all neofunctionalization processes undergo a

87 subfunctionalization transition state (Rastogi and Liberles, 2005).

88 If the mutations occur before the duplication event, as in allopolyploidy, the two variants

89 are unlikely to have degenerative mutations. Instead, they may have differing optimal condi-

90 tions in which they function or are expressed. The advantage of different variants at a single

91 locus (alleles; Allard and Bradshaw, 1964) or at duplicated loci (homeoalleles; Mac Key,

92 1970) can result in greater plasticity to environmental changes. Allopolyploidization has

93 been suggested as an evolutionary strategy to obtain the genic diversity necessary for inva-

94   sive plant species to adapt to the new environments they invade (Ellstrand and Schierenbeck,

95   2000; te Beest *et al.*, 2011).

96   Adams *et al.* (2003) showed that some homeoallelic genes in cotton were expressed in

97   an organ specific manner, such that expression of one homeolog effectively suppressed the

98   expression of the other in some tissues. These results have since been confirmed in other

99   crops such as wheat (Pumphrey *et al.*, 2009; Akhunova *et al.*, 2010; Feldman *et al.*, 2012;

100 Pfeifer *et al.*, 2014), and evidence for neofunctionalization of homeoallelic genes has been

101 observed (Chaudhary *et al.*, 2009). Differential expression of homeologous gene transcripts

102 has also been shown to shift upon challenge with heat, drought (Liu *et al.*, 2015) and salt

103 stress (Zhang *et al.*, 2016) in wheat, as well as water submersion and cold in cotton (Liu and

104 Adams, 2007).

105 Common wheat (*Triticum aestivum*) provides an example of an allopolyploid that has

106 surpassed its diploid ancestors in its value to humans as a staple source of calories. Hexaploid

107 wheat has undergone two allopolyploid events, the most recent of which occurred between

108 10 and 400 thousand years ago, adding the D genome to the A and B genomes (Marcussen

109 *et al.*, 2014). The gene diversity provided by these three genome ancestors may explain why

110 allohexaploid wheat has adapted from its source in southwest Asia to wide spread cultivation

111 around the globe (Dubcovsky and Dvořák, 2007; Feldman and Levy, 2012).

112 In the absence of outcrossing in inbred populations, selection can only act on individuals,

113 changing their frequency within the population. If the selection pressure changes (e.g. for

114 modern agriculture), combinations of homeoalleles within existing individuals may not be

115 ideal for the new set of environments and traits. This presents an opportunity for plant breed-

116 ers to capitalize on this feature of allopolyploids by making crosses to form new individuals

117 with complementary sets of homeoalleles. Many of these advantageous combinations have

118 likely been indirectly selected throughout the history of wheat domestication and modern

119 breeding.

120 Dominance of homeologous genes is known to exist in wheat. For example, a single

5

dominant red allele at any of the three homeologous kernel color genes on 3A, 3B, and 3D will confer a red kernel color (Allan and Vogel, 1965; Metzger and Silbaugh, 1970). Another crucial example involves the two homeologous dwarfing genes (Allan *et al.*, 1959; Gale *et al.*, 1975; Gale and Marshall, 1976; McVittie *et al.*, 1978) important in the Green Revolution, which implemented semi-dwarf varieties to combat crop loss due to nitrogen application and subsequent lodging. These genes have been shown to exhibit a quantitative semi-dominant reponse (Börner *et al.*, 1996). We discuss this example in detail, and use it as a starting point to justify the search for quantitative homeologous interactions genome-wide. While the effect of allopolyploidy has been demonstrated at both the transcript level and whole plant level, we are unaware of attempts to use genome-wide homeologous interaction predictors to model whole plant level phenotypes such as growth, phenology and grain yield traits.

Using a soft winter wheat breeding population, we demonstrate that epistatic interactions account for a significant portion of genetic variance and are abundant throughout the genome. Some of these interactions occur between homeoallelic regions and we demonstrate their potential as targets for selection. If advantageous homeoallelic interactions can be identified, they could be directly selected to increase homeoallelic diversity, with the potential to expand the environmental landscape to which a variety is adapted. We hypothesize that the presence of two evolutionarily divergent genes with partially redundant function leads to a less-than-additive gene interaction, and introduce this as a subfunctionalization model of epistasis.

3   Subfunctionalization Epistasis

We generalize the duplicate factor model of epistasis from Hill *et al.* (2008), by introducing a subfunctionalization coefficient s, that allows the interaction to shift between the duplicate factor and additive models. Let us consider an ancestral allele with an effect a. Through mutation, the effect of this locus is allowed to diverge from the ancestral allele to have effects $a^\star$ and $\tilde{a}$ in the two descendant species. When the two divergent loci are brought back
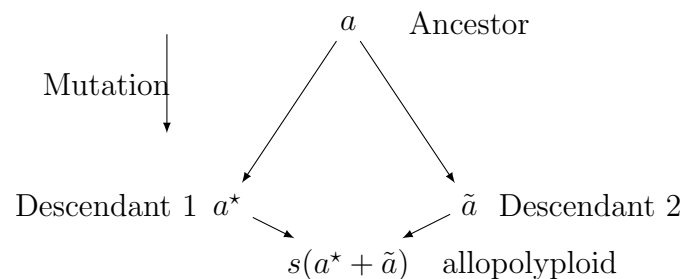
6

Mutation

a Ancestor

Descendant 1 $a^\star$

$\tilde{a}$ Descendant 2

$s(a^\star + \tilde{a})$ allopolyploid

Figure 1: Diagram of subfunctionalization where a is the effect of a functional allele, $a^\star$ and $\tilde{a}$ are the effects of the descendant alleles, and s is the subfunctionalization coefficient.

146 together in the same nucleus, the effect of combining these becomes $s(a^\star + \tilde{a})$ (Figure 1).

147 Values of $s < 1$, indicate a less-than additive epistasis (Eshed and Zamir, 1996), in this

148 case, resulting from redundant gene function. When $s = 1/2$, and $a^\star = \tilde{a}$, the descendant

149 alleles have maintained the same function and the duplicate factor model is obtained. As

150 s exceeds $1/2$, the descendant alleles diverge in function (i.e. subfunctionalization), until

151 s reaches 1, implying that the two genes evolved completely non-redundant function (i.e

152 neofunctionalization). At the point where $s = 1$, the effect becomes completely additive.

153 For values of $s > 1/2$, the benefit of multiple alleles is realized in a model analogous

154 to overdominance in traditional hybrids. As alleles diverge they can pick up advantageous

155 function under certain environmental conditions. The homeo-heterozygote then gains an

156 advantage if it experiences conditions of both adapted homeoalleles. Values of $s < 1/2$

157 may indicate allelic interference (Herskowitz, 1987), or genomic shock (McClintock, 1984),

158 a phenomenon that has been observed in many newly formed allopolyploids (Comai *et al.*,

159 2003). Allelic interference, also referred to as dominant negative mutation, can result from

160 the formation of non-functional homeodimers, while homodimers from the same ancestor

161 continue to function properly. This interference effectively reduces the number of active
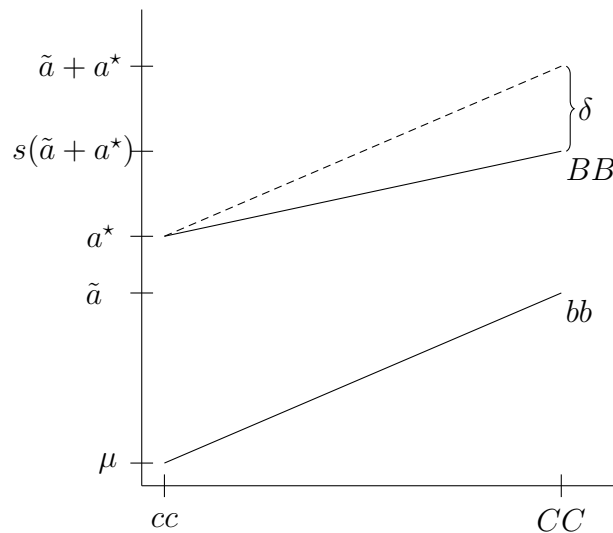
162 dimers by half (Herskowitz, 1987; Veitia, 2007).

7

Figure 2: Epistatic interaction of two loci, B and C, with the expected effects for the $\{0, 1\}$ parameterization. δ indicates the deviation of the $BBCC$ genotype from an additive model for the $\{0, 1\}$ parameterization, where $s = 1 + \frac{\delta}{\tilde{a} + a^\star}$. The dotted line indicates the expectation under the additive model.

3.1   Epistasis models

Let us consider the two locus model, with loci B and C. Using the notation of Hill *et al.* (2008), the expected phenotype, $\mathrm{E}[y]$, is modeled as

$$\mathrm{E}[y] = \mu + B\alpha_B + C\alpha_C + BC(\alpha\alpha)_{BC} \tag{1}$$

where B and C are the marker allele scores, BC is the pairwise product of those scores, α_B and α_C are the additive effects of the B and C loci and $(\alpha\alpha)_{BC}$ is the interaction effect.

We revisit two epistatic models, the "Additive $\times$ Additive Model without Dominance or Interactions Including Dominance" (called "Additive $\times$ Additive" hence forth) and the "Duplicate Factor" considered by Hill, Goddard and Visscher (Hill *et al.*, 2008) that are relevant for this discussion. Omitting the heterozygous classes and letting a be the effect on the phenotype,

8

Additive × Additive		
	CC	cc
BB	$2a$	0
bb	0	$2a$

Duplicate Factor		
	CC	cc
BB	a	a
bb	a	0

We propose a generalized Duplicate Factor epistatic model to estimate the degree of gene functional redundancy, or subfunctionalization.

Subfunctionalization		
	CC	cc
BB	$s(a^\star + \tilde{a})$	$a^\star$
bb	$\tilde{a}$	0

When markers are coded $\{0, 1\}$ for presence of the functional allele, the deviation from the additive expectation, δ, is estimated by $(\alpha\alpha)_{BC}$. δ can then be used to calculate the subfunctionalization coefficient, $s = 1 + \frac{\delta}{a^\star + \tilde{a}}$ (Figure 2). The least squares expectation of additive and epistatic effects is then

$$
\mathrm{E}\begin{bmatrix} \mu \\ B\alpha_B \\ C\alpha_C \\ BC(\alpha\alpha)_{BC} \end{bmatrix} = \begin{bmatrix} \mu \\ a^\star \\ \tilde{a} \\ \delta \end{bmatrix} = \begin{bmatrix} \mu \\ a^\star \\ \tilde{a} \\ (d-1)(a^\star + \tilde{a}) \end{bmatrix}
$$

3.2 Epistatic contrasts

Epistatic interaction predictors must be formed from marker scores in order to estimate interaction parameters. These interaction predictors are typically calculated as the pairwise product of the genotype scores for their respective loci. This can lead to ambiguity in the meaning of those interaction effects depending on how the marker scores are coded. Different marker parameterizations can center the problem at different reference points (i.e. different intercepts), and can scale the predictors based on allele or genotype effects (i.e. different slopes).

9

Table 1: Epistatic interaction score tables resulting from the products of marker scores using $\{-1, 1\}$ and $\{0, 1\}$ parameterizations for inbreds.

	CC	cc		CC	cc
BB	1	-1	BB	1	0
bb	-1	1	bb	0	0

189   When loci B and C are coded as $\{-1, 1\}$ for inbred genotypes, including the product of

190   the marker scores, BC, corresponds to the Additive $\times$ Additive model (Table 1). Changing

191   the reference allele at either locus does not change the magnitude of effect estimates but

192   will change their signs. Using $\{0, 1\}$ coding, BC corresponds to the subfunctionalization

193   model and estimates δ directly. For this coding scheme, the magnitude and sign can change

194   depending on the reference allele at the two loci. This highlights one of the difficulties of

195   effect interpretation, as it is not clear which marker orientations should be paired. That is,

196   which allele should be B as opposed to b, and which should be C as opposed to c? Marker

197   alleles can be oriented to have either all positive or all negative additive effects, but the

198   question remains: which direction should the more biologically active allele have on the

199   phenotype?

200   Marker scores are typically assigned as either presence (or absence) of the reference,

201   major, or minor allele, which may or may not be biologically relevant. While it has been

202   noted that the two different marker encoding methods do not result in the same contrasts

203   of genotypic classes (He *et al.*, 2015; Martini *et al.*, 2016, 2017), coding does not affect the

204   least squares model fit (Zeng *et al.*, 2005; Álvarez-Castro and Carlborg, 2007). Álvarez-

205   Castro and Carlborg (2007) show that there exists a linear transformation to shift between

206   multiple parameterizations using a change-of-reference operation (see Appendix 3). This is

207   convenient because all marker orientation combinations can be easily generated by changing

208   the effect signs of a single marker orientation fit for the $\{-1, 1\}$ marker coding. These effect

209   estimates can subsequently be transformed to the $\{0, 1\}$ coding effect estimates using the

210   change-of-reference operation for all marker orientation combinations.

211   This transformation does not hold when marker effects are considered random, where

10

the interaction effect is subject to differential shrinkage depending on the marker coding and orientation (Martini *et al.*, 2017, 2018). As such, orienting markers to capture functional allele relationships may be crucial for optimizing genomic prediction including epistasis. We make an attempt to orient markers based solely on estimated fixed marker additive effects, with the assumption that that homeoalleles with similar additive effects are functionally similar. Other attempts at marker orientation have included orienting markers to maximize the interaction effect magnitude and including interaction predictors from all possible marker orientations (Martini *et al.*, 2017). The former is biased toward selecting interaction predictors with a high joint frequency, whereas the latter suffers from a high degree of linear dependency.

4 Materials and Methods

4.1 RIL population

A bi-parental recombinant inbred line (RIL) population of 158 lines segregating for two dwarfing genes was used to illustrate an epistatic interaction between the well known homeologous genes on chromosomes 4B and 4D, *Rht-B1* and *Rht-D1*, important in the Green Revolution (Allan *et al.*, 1959; Gale *et al.*, 1975; Gale and Marshall, 1976; McVittie *et al.*, 1978). Two genotyping by sequencing (GBS) markers linked to these genes were used to track the segregating mutant (*b* and *d*) and wildtype (*B* and *D*) alleles. Only one test for epistasis between these two markers was run. This homeologous marker pair was denoted RIL_Rht1. Details of the population can be found in Appendix 1.

4.2 CNLM population

The Cornell small grains soft winter wheat breeding population (CNLM) was used to investigate the importance of homeologous gene interactions in a large adapted breeding population. The dataset and a detailed description of the CNLM population can be found in Santanto-

11

236 nio *et al.* (2018b). Briefly, the dataset consists of 1,447 lines evaluated in 26 environments

237 around Ithaca, NY. Because the data were collected from a breeding population, only 21% of

238 the genotype/environment combinations were observed, totaling 8,692 phenotypic records.

239 Standardized phenotypes of four traits, grain yield (GY), plant height (PH), heading date

240 (HD) and test weight (TW) were recorded. All lines were genotyped with 11,604 GBS mark-

241 ers aligned to the International Wheat Genome Sequencing Consortium (IWGSC) RefSeq

242 v1.0 wheat genome sequence of 'Chinese Spring' (IWGSC, 2018, accepted), and subsequently

243 imputed.

4.3   Homeologous marker sets

245 Using the IWGSC RefSeq v1.0 'Chinese Spring' wheat genome sequence (IWGSC, 2018,

246 accepted), homeologous sets of genes were constructed by aligning the annotated coding

247 sequences (v1.0) back onto themselves. The known 4A, 5A, and 7B translocation in wheat

248 (Devos *et al.*, 1995) was ignored for simplicity in this study, but could easily be accounted for

249 by allowing homeologous pairs across these regions. The resulting 23,796 homeologous gene

250 sets, comprised of 18,184 triplicate and 5,612 duplicate gene sets, sampled roughly 59% of

251 the gene space of hexaploid wheat. Additional details on homeologous gene alignment can be

252 found in Appendix 2. Each homeologous gene was then anchored to the nearest marker by

253 physical distance (Supplementary Figures S1 and S2), and homeologous sets of markers were

254 constructed from the anchor markers to each homeologous gene set. Redundant marker sets

255 due to homeologous genes anchored by the same markers were removed, resulting in 6,142

256 triplicate and 3,985 duplicate marker sets for a total of 10,127 unique homeologous marker

257 sets. These marker sets (denoted 'Homeo') were then used to calculate marker interaction

258 scores as pairwise products of the marker score vectors.

259 As a control, two additional marker sets were produced by sampling the same number

260 of duplicate and triplicate marker sets as the Homeo set. These markers sets were sampled

261 either from chromosomes within a subgenome (Within, e.g. markers on 1A, 2A and 3A), or

12

262 across non-syntenic chromosomes of different subgenomes (Across, e.g. markers on 1A, 2B

263 and 3D). Samples were taken to reflect the same marker distribution of the Homeo set with

264 regard to their native genome, which has a larger proportion of D genome markers relative

265 to their abundance. Note that three-way homeologous interactions have equal proportions

266 of markers belonging to the A, B and D genomes, whereas D genome markers only account

267 for 13% of all markers in the CNLM population (Santantonio *et al.*, 2018b).

4.4 Determining marker orientation

269 For each homeologous marker set, additive homeologous marker effects and their multiplica-

270 tive interaction effects were estimated as fixed effects in the following linear mixed model

271 while correcting for background additive and epistatic effects. The $\{-1, 1\}$ marker parame-

272 terization was used for fixed marker additive and interaction effect estimates.

$$\mathbf{y} = \tilde{\mathbf{Z}}\mathbf{S}_{\text{-}11}\mathbf{E}_{\text{-}11} + \mathbf{X}\boldsymbol{\beta} + \mathbf{Z}\mathbf{g}_{G+I} + \boldsymbol{\varepsilon} \tag{2}$$

273 where $\mathbf{X}$ is the design matrix, $\boldsymbol{\beta}$ is the vector of fixed environmental effects, and $\mathbf{Z}$ is the

274 line incidence matrix. $\mathbf{S}_{\text{-}11}$ is the matrix of genotype marker scores and interactions for

275 each genotype class, while $\mathbf{E}_{\text{-}11}$ is the fixed additive and interaction effects that need es-

276 timated (Appendix 3). $\tilde{\mathbf{Z}}$ is the incidence matrix for the two- or three-way genotype of

277 each homeologous marker set. $\mathbf{Z}$ and $\tilde{\mathbf{Z}}$ differ in that the former links observations to a

278 specific line, whereas the latter links observations to one of the two- or three-way genotype

279 classes for the homeologous marker set. The background genetic effects were assumed to

280 be $\mathbf{g}_{G+I} \sim \mathcal{N}(0, \sigma_G^2 \mathbf{K}_G + \sigma_I^2 \mathbf{H}_I)$ with population parameters previously determined (Zhang

281 *et al.*, 2010). The additive and epistatic covariances, $\mathbf{K}_G$ and $\mathbf{H}_I$, were calculated as de-

282 scribed in VanRaden (2008, method I) and Martini *et al.* (2016, equation 9), respectively.

283 This weighted covariance matrix was used to reduce computational burden associated with

284 estimating two variance components in the same fit.

13

285   A Wald test was used to obtain a p-value for marker additive and interaction effects.

286 All marker orientation combinations were generated by changing the estimated effect signs,

287 and then transformed to the $\{0, 1\}$ marker effect estimates using the change-of-reference

288 operation (Álvarez-Castro and Carlborg, 2007). Only marker orientations with all positive

289 or all negative additive effects were considered. It should be noted that the marker orientation

290 has no effect on the p-value, as they are linear transformations of one another.

291   Markers were oriented to have minimized the difference (or variance for three-way sets)

292 of the additive main effects while maximizing the mean of the absolute values of the additive

293 main effects. This orientation, which we denote 'low additive variance high additive effect'

294 (LAVHAE), assumes that marker alleles with similar effects are functionally similar. Only

295 additive effects were used to select the marker orientation to keep from systematically select-

296 ing marker orientations with a specific interaction pattern. Three other marker orientation

297 schemes were also investigated by orienting markers to either have all positive (POS) effects,

298 all negative (NEG) effects, or to maximize the variance of the additive and interactions

299 effects ('high total effect variance', HTEV).

4.5   Additive only simulated controls

301 Marker effect and interaction estimates using either $\{0, 1\}$ or $\{-1, 1\}$ marker parameter-

302 izations are not orthogonal, so care must be taken when interpreting the direction and

303 magnitude of the effects estimates. The positive covariance between the marker scores and

304 their interaction leads to a multicollinearity problem, and results in a negative relationship

305 between additive and interaction effects if both additive effects are oriented in the same

306 direction. To determine if the negative relationship between the additive and epistatic ef-

307 fects was greater than expected due to multicollinearity, a new phenotype with no epistatic

308 effects was simulated from the data for each trait. The estimate of the marker variance was

309 calculated from the additive genetic variance estimate as $\hat{\sigma}_m^2 = \hat{\sigma}_G^2 (2\mathbf{p}^{\mathrm{T}}(\mathbf{1} - \mathbf{p}))^{-1}$, where

310 $\mathbf{p}$ is the vector of marker allele frequencies. Then for each trait, a new additive phenotype

³¹¹ was simulated as $\mathbf{y}_{sim} = \mathbf{1}\mu + \mathbf{X}\hat{\boldsymbol{\beta}} + \mathbf{ZMu}_{sim} + \boldsymbol{\varepsilon}_{sim}$ where the trial effect estimates from

³¹² Santantonio *et al.* (2018b, equation 2) were used for $\hat{\boldsymbol{\beta}}$, $\mathbf{M}$ is the matrix of marker scores,

³¹³ $\mathbf{u}_{sim}$ was sampled from $\mathcal{N}(0, \hat{\sigma}_m^2)$ and $\boldsymbol{\varepsilon}$ was sampled from $\mathcal{N}(0, \hat{\sigma}^2)$. A Kolmogorov-Smirnov

³¹⁴ (KS) test was used to determine if the distribution of the estimated interaction effects from

³¹⁵ the actual data differed from the distribution of effects estimated from simulated data. An

³¹⁶ additional simulated phenotype was also produced by first permuting each column of $\mathbf{M}$ to

³¹⁷ remove any effects due to linkage disequilibrium (LD) structure.

4.6   Genomic prediction

³¹⁹ To determine the importance of epistatic interactions to the predictability of a genotype, a

³²⁰ genomic prediction model was fit as

$$\mathbf{y} = \mathbf{1}\mu + \mathbf{X}\boldsymbol{\beta} + \mathbf{Zg}_G + \mathbf{Zg}_I + \boldsymbol{\varepsilon} \tag{3}$$

³²¹ where $\mathbf{1}_n$ is a vector of ones, μ is the general mean. The random vectors of additive genotype,

³²² epistatic interactions, and errors were assumed to be distributed as $\mathbf{g}_G \sim \mathcal{N}(0, \sigma_G^2 \mathbf{K})$, $\mathbf{g}_I \sim$

³²³ $\mathcal{N}(0, \sigma_I^2 \mathbf{H})$ and $\boldsymbol{\varepsilon} \sim \mathcal{N}(0, \sigma^2)$, respectively.

³²⁴   The additive covariance matrix, $\mathbf{K}$, was calculated using VanRaden (2008), method I.

³²⁵ The epistatic covariance matrix $\mathbf{H}$ was calculated either as defined by Jiang and Reif (2015,

³²⁶ equation 5) and Martini *et al.* (2016, equation 9) to model all pairwise epistatic interactions

³²⁷ using $\{-1, 1\}$ coding (Pairwise), or in a similar fashion as $\mathbf{K}$ for oriented marker sets, where

³²⁸ only unique products of marker variables were included instead of the marker variables. For

³²⁹ the latter, the matrix was scaled with the sum of the joint marker variances as $(2\mathbf{q}^{\mathrm{T}}(\mathbf{1} - \mathbf{q}))^{-1}$,

³³⁰ where $\mathbf{q}$ is the joint frequency of individuals containing both the non-reference marker alleles.

³³¹ Three-way marker products were included if they were unique from the additive and pairwise

³³² product predictors.

³³³   A small coefficient of 0.01, was added to the diagonals of the covariance matrix to recover

334 full rank lost in centering the matrix of scores prior to calculating the covariance. Five-fold

335 cross validation was performed by randomly assigning individuals to one of five folds for

336 10 replications. Four folds were used to train the model and predict the fifth fold for all

337 five combinations. All models were fit to the same sampled folds so that models would

338 be directly comparable to one another and not subject to sampling differences. Prediction

339 accuracy was assessed by collecting genetic predictions for all five folds, then calculating the

340 Pearson correlation coefficient between the predicted genetic values for all individuals and a

341 "true" genetic value. The "true" genetic values were obtained by fitting a mixed model to

342 all the data with fixed effects for environments and a random effect for genotypes, assuming

343 genotype independence with a genetic covariance $\mathbf{I}$.

344   Increase in genomic prediction accuracy from the additive model was used as a proxy

345 to assess the relative importance of oriented marker interaction sets. To determine the

346 proportion of non-additive genetic signal attributable to each interaction set, the ratio of

347 the prediction accuracy increase from the additive model using the interaction set (Homeo,

348 Within and Across) to the prediction accuracy increase from the additive model modeling all

349 pairwise epistatic interactions (Pairwise) was used for comparison of models. The percentage

350 of non-additive predictability was calculated as follows for each interaction set.

$$\frac{\text{accuracy(Interaction Set)} - \text{accuracy(Additive)}}{\text{accuracy(Pairwise)} - \text{accuracy(Additive)}} \quad (4)$$

351 ## 4.7   Software

352 ASReml-R (Gilmour, 1997; Butler, 2009) was used to fit all mixed models. BLAST+ (Ca-

353 macho *et al.*, 2009) was used for coding sequence alignment. All additional computation,

354 analyses and figures were made using base R (R Core Team, 2015) implemented in the Mi-

355 crosoft Open R environment 3.3.2 (Microsoft, 2017) unless noted otherwise. Figures 1 and

356 2 were created using the 'tikz' package (Tantau, 2018) for LaTeX. Figure 4 was made with

357 the 'circlize' R package (Gu *et al.*, 2014). The R package 'xtable' (Dahl, 2016) was used to

16

Table 2: Marker and epistatic effect estimates for *Rht-1D* and *Rht-1B* linked GBS markers for plant height (cm) in 158 RIL lines derived from NY91017-8080 $\times$ Caledonia. Least squares effect estimates are for markers coded either using $\{0, 1\}$ coding or $\{-1, 1\}$, and then oriented such that the two marker main effects are either both positive $(+)$ or both negative $(-)$.

Marker Coding	Effect Orientation	Intercept	*Rht-1B*	*Rht-1D*	*Rht-1B*$\times$*Rht-1D*	s^a
$\{0, 1\}$	$+$	69.9	23.4	22.2	-12.2	0.73
$\{0, 1\}$	$-$	103.3	-11.2	-10.0	-12.2	1.58
$\{-1, 1\}$	$+$	89.7	8.6	8.0	-3.0	
$\{-1, 1\}$	$-$	89.7	-8.6	-8.0	-3.0	

[a]The subfunctionalization coefficient calculated from the additive and interaction effects is shown for the $\{0, 1\}$ marker coding.

358 generate LaTeX tables in R.

4.8 Data availability

360 Phenotypes and genotypes for the CNLM population can be found in Santantonio *et al.*

361 (2018b). A list of homeologous genes can be found in supplementary file 'homeoGeneList.txt'.

362 The supplementary file 'HomeoMarkerSet.txt' contains non-unique marker sets anchored to

363 each homeologous gene set. Unique marker sets used can be found in 'uniqueHomeoMark-

364 erSet.txt', 'WithinMarkerSet.txt', 'AcrossMarkerSet.txt' for the Homeo, Within and Across

365 marker sets. Marker and marker interaction effect estimates and p-values for the Homeo set

366 can be found in 'twoWayInteractions.txt' and 'threeWayInteractions.txt' for two- and three-

367 way marker interactions, respectively. Phenotypes and genotypes used in the RIL population

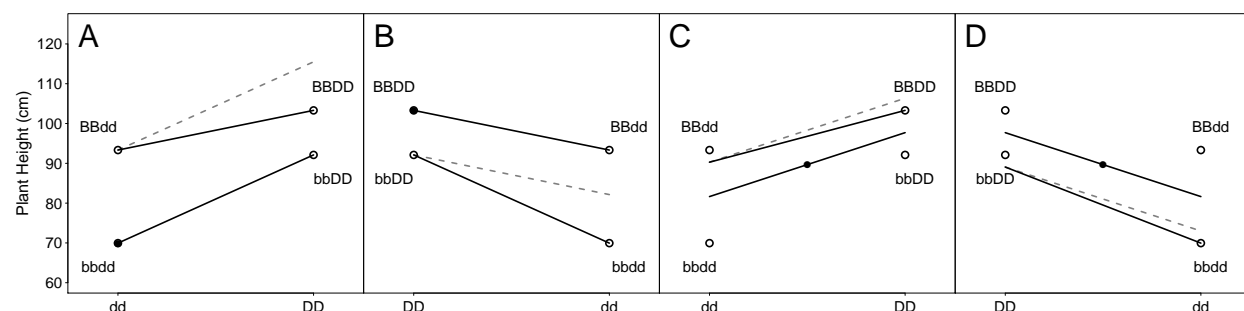368 are included in the 'NY8080Cal.txt' file.

17

Figure 3: Epistasis plot of effects for *Rht-1B* and *Rht-1D* linked markers on plant height in 158 RIL lines derived from NY91017-8080 × Caledonia. The filled circles indicate the intercept (i.e. reference point) for each model parameterization while open circles indicate genotype class means. The solid lines indicate the marker effect estimates including the interaction term, while the dotted line indicates the expectation based on the additive model. **A**) $\{0, 1\}$ marker coding with positive marker effect orientation. **B**) $\{0, 1\}$ marker coding with negative marker effect orientation. **C**) $\{-1, 1\}$ marker coding with positive marker effect orientation, **D**) $\{-1, 1\}$ marker coding with negative marker effect orientation.

5 Results and Discussion

5.1 Rht-1

5.1.1 RIL population

The markers linked to the *Rht-1B* and *Rht-1D* genes both had significant additive effects (p $< 10^{-10}$) and explained 19.6% and 20.5% of the variation in the height of the RIL population (Supplemental Table S1). The test for a homeoallelic epistatic interaction between these *Rht-1* linked loci was also significant (p = 0.0025), but only explained 3.5% of the variance after accounting for the additive effects. Had we tested all pairwise marker interactions in this population, this test would not have passed a Bonferroni corrected significance threshold.

Effect estimates for the *Rht-1* markers and their epistatic interaction are shown in Table 2, for $\{0, 1\}$ and $\{-1, 1\}$ marker parameterizations, and for orientations where the marker main effects are both positive or both negative. The $\{0, 1\}$ parameterization is arguably more intuitive, as effects correspond directly to differences in genotype values (Figure 3). They both contain the same information and are equivalent for prediction using ordinary

18

383 least squares, but the interpretation of the $\{-1, 1\}$ marker coding is less obvious because
384 the slopes are deviations from the expected double heterozygote (assuming no dominance),
385 which does not exists in an inbred population. The $\{0, 1\}$ parameterization uses the double
386 dwarf as the reference point, where the effects α_B and α_C are the two semi-dwarf genotypes.
387 The tall genotype is the sum of the semi-dwarf allele effects plus the deviation coefficient, δ,
388 which corresponds to $(\alpha\alpha)_{BC}$.

389 The estimated s parameter of 0.73 indicates a significant degree of redundancy between
390 the wild type *Rht-1* homeoalleles. This suggests that either the gene products maintain par-
391 tial redundancy in function, or the expression of the two homeoalleles is somewhat redundant.
392 The latter is less likely given that the two functional wild type genes have comparable addi-
393 tive effects relative to the double dwarf. If the two genes were expressed at different times or
394 in different tissues based on their native subgenome, the additive effects would be likely to
395 differ in magnitude. This demonstrates a functional change between homeoalleles that has
396 been exploited for a specific goal, semi-dwarfism.

397 When the markers are oriented in the opposite direction, to indicate the GA insensitive
398 mutant allele as opposed to the GA sensitive wildtype allele, the interpretation of the in-
399 teraction effect changes. The additive effect estimates become indicators of the reduction in
400 height by adding a GA insensitive mutant allele. The interaction effect becomes the addi-
401 tional height reduction from the additive expectation of having both GA insensitive mutant
402 alleles, resulting in a s parameter of 1.58. The same interpretation can be made, but must
403 be done so with care. Losing wildtype function at both alleles results in a more drastic
404 reduction in height than expected because there is redundancy in the system. Therefore, the
405 s parameter is most easily interpreted when the functional direction of the alleles is known.
406 Simply put, when function is added on top of function, little is gained, but when all function
407 is removed, catastrophe ensues.

19

5.1.2 CNLM population

For the CNLM population, the markers with the lowest p-values associated with plant height on the short arms of 4B and 4D did not show a significant interaction with their respective assigned homeologous marker in homeologous sets H4.16516 and H4.23244, respectively. A new homeologous marker set, CNLM_Rht1, was constructed with the SNPs on 4BS and 4DS with the lowest p-values mentioned above. The additive effects of markers S4B_PART1_38624956 and S4D_PART1_10982050 had p-values of 5.5×10^{-4} and 3.7×10^{-8}, respectively, while the interaction had a p-value of 0.015. This set was oriented in the same direction as the RIL_Rht1 set using the LAVHAE orientation method. While the magnitude of these effects was reduced (7.13, 7.09 and -4.56 for the 4D, 4B and 4B×4D effects respectively), the CNLM_Rht1 set had a s parameter value of 0.68, similar to that of RIL_Rht1. Had this set alone been tested, we would have concluded that this was a significant homeologous interaction.

To verify these results, we genotyped 1,259 individuals of the CNLM population with two 'perfect' markers designed to track the *Rht-1B* and *Rht-1D* alleles (Ellis *et al.*, 2002). When correcting for population structure, effect estimates were 1.66 (p $= 3.3 \times 10^{-2}$), 1.93 (p $< 2 \times 10^{-16}$) and -1.02 (p $= 6.4 \times 10^{-6}$) for the *Rht-1B Rht-1B* and *Rht-1B* × *Rht-1B* terms, respectively, resulting in an s value of 0.71. The relatively high p-value for the *Rht-1B* is likely due to correction for population structure, where the *Rht-1Db* dwarfing allele is the predominant source of semi-dwarfism in the breeding population (Supplementary Table S3). Ignoring population structure produced p-values of p $< 10^{-19}$ for both additive effects and p $= 5.7 \times 10^{-5}$ for the interaction.

5.2 Significant homeoallelic interactions

The absence of one genotype class in 7,912 interaction terms resulted in 20,641 testable interaction effects out of 28,553 total interaction terms. A trait-wise Bonferroni significance threshold of $0.05/20,641 = 2.4 \times 10^{-6}$ was therefore used to determine which interaction ef-
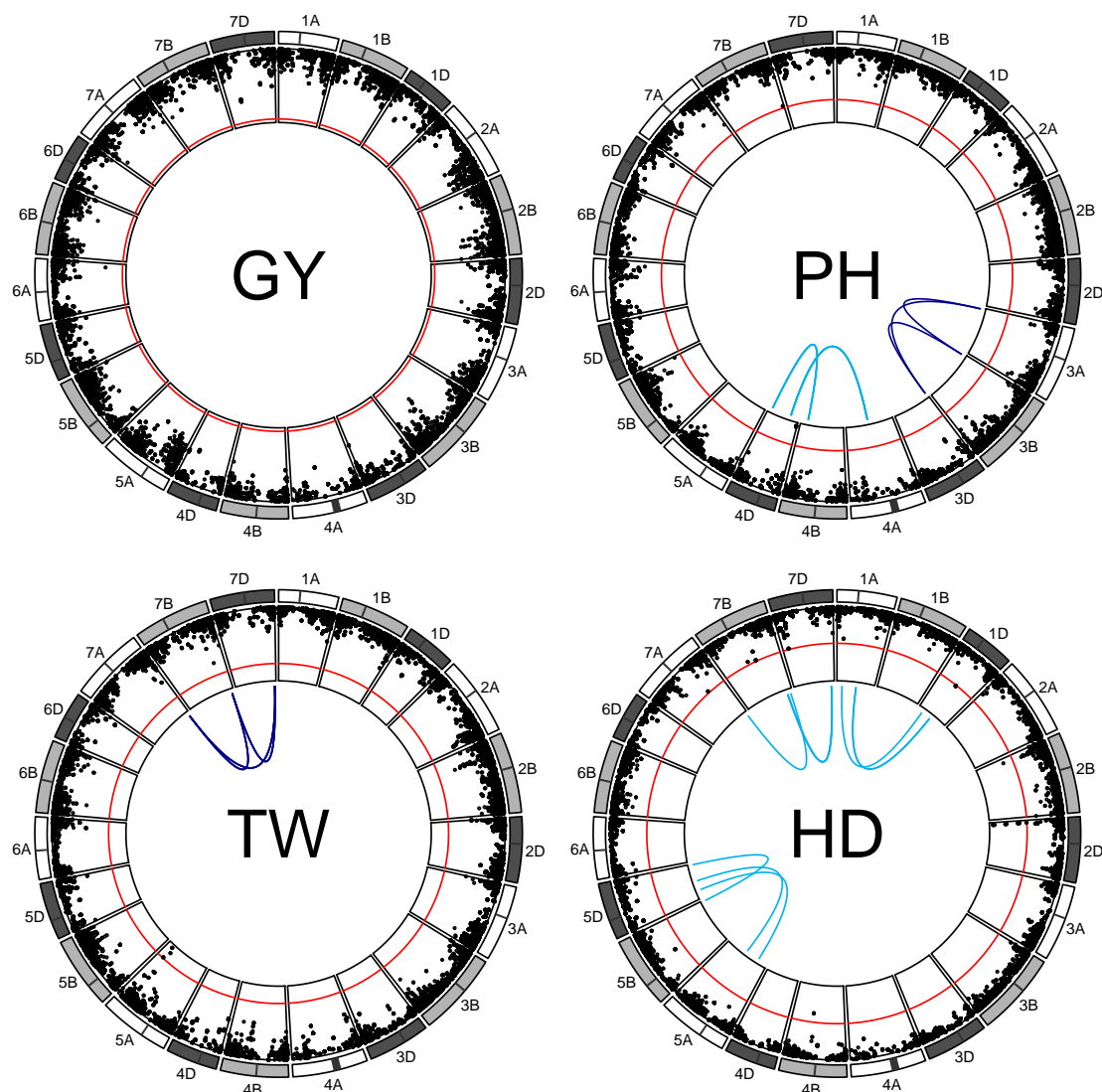
20

Figure 4: Manhattan plot of homeoallelic marker sets for each of the 21 chromosomes of wheat. The red line indicates a trait wise Bonferroni significance threshold for additive effects of $-\log_{10}(6.0 \times 10^{-6}) = 5.2$. Light blue lines indicate significant two-way homeoallelic marker interactions that exceeded a Bonferroni threshold for all testable interaction effects $-\log_{10}(2.4 \times 10^{-6}) = 5.6$. Dark blue lines indicate significant 3-way homeoallelic marker interactions that exceeded the same Bonferroni threshold.

434 fects had a significant effect on the phenotype. Few homeoallelic interactions were significant

435 at the trait-wise Bonferroni cutoff (Figure 4). Significant homeoallelic interactions for PH

436 were identified between 4AL and 4DS, as well as 4BL and 4DL. Both of these locations were

437 likely too far away from the *Rht-1* alleles to be tagging these genes directly, but they may

438 be regulatory sites for these genes. Another set of interacting sites between the homeologous

21

439 chromosome arms 3AS, 3BS and 3DS was also identified for PH, but the additive effects were
440 not significant. Two interacting regions on homeolog 1, between 1AS and 1DS and between
441 1AL and 1DL, and three interacting regions on homeolog 5 also appeared to be influencing
442 HD. One region on the distal end of homeolog 7 affected both HD and TW, with significant
443 two-way and three-way interactions. Although they were tagged with different marker sets
444 for the two traits, these epistatic regions appeared to co-localize within 2 Mbp.

445   No significant additive or interaction effects were detected for GY, highlighting the highly
446 polygenic nature of the grain yield trait. In several cases, one of the additive effects was
447 significant but the other was not, and it is not clear if this is influencing the detection of
448 interactions. It may be that the significant marker is simply in higher LD with the functional
449 mutation conditional on the presence of the other marker, allowing the interaction to pick
450 up the additional signal from the functional mutation (Wood *et al.*, 2014). However, if this
451 were the case, the interaction would be expected to be in the same direction as the additive
452 effect, which was not generally observed.

453   We did not detect an interaction between the two significant additive regions on 2B
454 and 2D for the HD trait. While these two markers were not grouped as a homeologous
455 set, they were tested as such based on their proximity to the well described Photoperiod-1
456 genes, *Ppd-B1* and *Ppd-D1*, on chromosomes 2B and 2D respectively. These genes are known
457 to influence photoperiod sensitivity, and therefore transition to flowering and heading date
458 (Welsh J.R. and R.D., 1973; Law *et al.*, 1978; Scarth and Law, 1983). Certain allele pairs
459 at these genes have been shown to exhibit a high degree of epistasis (Poland, 2018, personal
460 communication) in a bi-parental family. It is unclear why no interaction was observed in
461 this population.

462   Jiang *et al.* (2017) also investigated the presence of homeologous interactions, but found
463 little evidence in a large population of hybrid wheat. They did not attempt to tag homeol-
464 ogous loci, but instead considered interactions across any markers on homeologous chromo-
465 somes to be syntenic. Interactions at homologous and non-homeologous loci may have largely

22

466 outweighed interactions across homeologous loci in that population, given it was constructed

467 from highly divergent parents and that progeny were not inbred. Additionally, they tested

468 all pairwise marker combinations, resulting in a strict significance threshold that may have

469 missed small effect homeologous interactions.

470 Homeologous interactions make up relatively few of the potential two-way interactions

471 within an allopolyploid genome. Given a subgenome with k genes and alloploidy level p

472 (i.e. the number of subgenomes), there are $k\binom{p}{2}$ two-way homeologous interactions versus

473 $\binom{kp}{2} - k\binom{p}{2}$ potential two-way non-homeologous gene interactions. For a subgenome size of

474 30,000 genes, this represents 0.02% and 0.006% of the possible two-way gene interactions

475 for an allotetraploid and an allohexaploid, respectively. That said, homeoallelic interactions

476 should be far more likely to have a true biological interaction than random pairs of genes

477 because they should belong to the same or similar biochemical pathways.

5.3 Estimates of the subfunctionalization coefficient

479 There were few cases where at least two additive effects and their corresponding interaction

480 effect were all significantly different from zero. This may be due to the difficulty of assigning

481 functional homeologous gene sets using single SNPs, as well as a lack of statistical power

482 owing to low minor allele frequencies (Hill *et al.*, 2008). The lack of a large number of

483 significant interactions is not surprising given that allele frequencies near 0.5 are uncommon

484 in both natural and breeding populations.

485 To determine whether more homeologous marker sets were displaying a pattern indicative

486 of subfunctionalization than would be expected by chance, marker sets where both additive

487 and two-way interaction effects were significant at a threshold of $\alpha = 0.05$ were examined

488 (Table 3). The expected number of two-way marker sets with significant additive and in-

489 teraction effects is about 11 (i.e. 4 traits $\times$ 22,411 two-way interactions $\times$ 0.05^3), assuming

490 independence of loci and true additive and interaction effects of zero. Only the Homeo and

491 Across marker sets had significantly more than expected. When broken down by trait, these
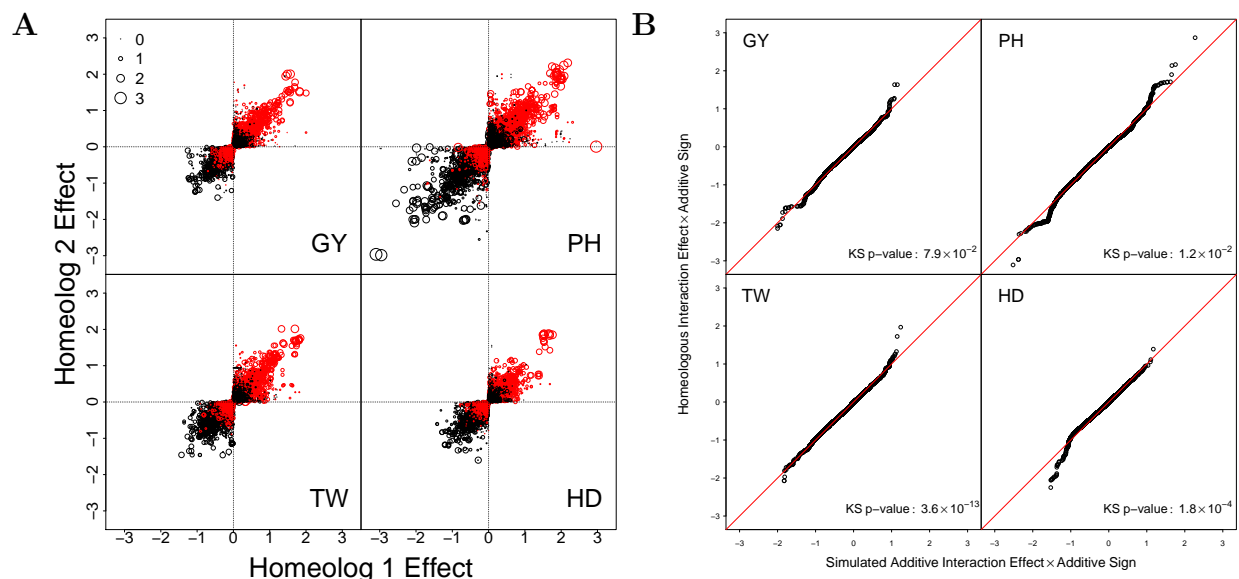
23

Figure 5: **A**) LAVHAE oriented homeologous marker pair additive effects for four traits, GY, PH, TW and HD. Point size represents the magnitude of the two-way homeologous interaction effect while color denotes the direction of the interaction effect, where black is positive and red is negative. **B**) Quantile quantile plot of the ordered estimated homeologous interaction effects plotted against those from a simulated phenotype sampled to obtain no epistatic interactions. Interaction effects have been multiplied by the effect sign of the corresponding additive effects to emphasize the relationship between the additive and interaction effects. The lower left quadrant indicates a less-than-additive interaction, whereas the upper right quadrant indicates a greater-than-additive interaction. The p-value from a Kolmorgorov-Smirnov (KS) test is reported to test if the distributions of actual and simulated interaction effect estimates are the same. A deviation below the line on the bottom left of each graph (i.e. a low dropping tail) should indicate a less-than-additive epistatic pattern of subfunctionalization, whereas a deviation above the line in the upper right (i.e. a high rising head) should indicate a greater-than-additive epistasis pattern of homeologous overdominance.

appeared to be driven by interactions for PH and TW in the Homeo set (Supplementary Table S16). The homeologous marker set had a larger proportion of s coefficients estimated between 0.5 and 1 relative to the strictly additive simulated phenotypes as well as the other non-homeologous marker sets, suggesting that homeologous loci exhibit a pattern indicative of subfunctionalization more so than other marker sets tested. The Across set showed the highest proportion of $s < 0.5$, suggestive of gene pathway interference. Because the power to detect significant effects diminishes as more tests are accomplished, it may be prudent to look at global trends between homeologous additive effects and their interactions, regardless

24

Table 3: Estimates of s coefficients for marker sets where both additive and the two-way interaction effects were significant at $p < 0.05$, combined for all 4 traits. The expected number of non-zero additive and two-way interactions effects based on a 0.05 significance threshold by chance is 11 (i.e. 4 traits $\times$ 22,411 two-way interactions $\times$ 0.05^3). Coefficients have been grouped by categories related to the potential mode of epistasis, where $s < 0.5$ indicates a highly negative interaction, $0.5 \leq s < 1$ a less-than-additive interaction may be indicative of subfunctionalization for homeologous genes, and $s > 1$ which indicates positive, or greater-than-additive, epistasis. Three marker sets are shown, either across all homeologous loci (Homeo), sampled sets within (Within) and across (Across) non-syntenic subgenome regions. An additional phenotype was simulated to contain additive only phenotypes to contain no epistasis, and fit with the Homeo marker set (Simulated Additive).

Marker Set	$s < 0.5$	$0.5 \leq s < 1$	$s > 1$	Total[a]
Homeo	8	14	8	30***
Simulated Additive	1	1	4	6
Across	9	7	1	17*
Within	6	3	4	13

[a]*, **, *** indicate significantly greater than the expected number of significant sets at p = 0.05, 0.01 and 10^{-6} based the binomial distribution with 89,644 trials and a probability of 0.05^3.

of statistical significance.

5.4   Evidence of subfunctionalization

A strong negative relationship between additive and interaction effects was observed when using the $\{0,1\}$ marker parameterization (Figure 5A). This negative relationship was also observed in the phenotypes simulated to be strictly additive (Supplementary Figure S3). The multicollinearity of the additive and epistatic predictors at least partially drives this relationship, where positively correlated additive and epistatic predictors will tend to have effect estimates in opposing directions.

To determine if the interaction effects were greater in magnitude than expected by chance, the ordered interaction effects from the true and simulated phenotypes were plotted against one another to form a quantile-quantile plot (Figure 5B). The interaction effects were multiplied by the sign of the corresponding additive effects to highlight the direction of interaction effect relative to the additive effect. Interaction effect distributions were significantly

⁵¹³ different between the observed and strictly additive simulated data as determined by the

⁵¹⁴ Kolmogorov-Smirnov test (KS; $p < 0.05$) for all traits except GY.

⁵¹⁵ HD showed a pattern consistent with a subfunctionalization model, with a low dropping

⁵¹⁶ tail for interaction effects in the opposite direction than that of the corresponding additive

⁵¹⁷ effects. This indicates that the less-than-additive effects of some estimated interactions are

⁵¹⁸ greater than expected by additivity alone. PH showed some evidence of this pattern, but

⁵¹⁹ also demonstrated a greater-than-additive effect for positively related interaction effects. The

⁵²⁰ LAVHAE orientation scheme may have selected the wrong marker coding for those marker

⁵²¹ sets, resulting in a s parameter greater than 1, or there are true greater-than-additive interac-

⁵²² tion responses for positive effect alleles. Greater than additive responses would be indicative

⁵²³ of overdominance across homeologous loci. GY and TW showed little evidence of the less-

⁵²⁴ than-additive pattern, yet TW did show this trend when the HTEV marker orientation was

⁵²⁵ used (Supplemental Figures S5 and S6). These relationships were more pronounced when

⁵²⁶ the markers were permuted to remove LD before simulating the data (Supplemental Figure

⁵²⁷ S4). High LD between homeologous marker sets may result in dampening of the epistatic

⁵²⁸ signal due to unbalanced or missing genotype classes.

⁵²⁹ These findings are further supported by comparing the homeologous interactions to the

⁵³⁰ Within and Across interaction effect estimates. The Homeo marker set showed more severe

⁵³¹ less-than-additive epistasis than both Within and Across for HD but not the other traits

⁵³² (Supplementary Figures S7 and S8). The Within set had more severe less-than-additive

⁵³³ interaction effects than the Homeo set for TW (Supplementary Figure S7), and the Across

⁵³⁴ had more severe less-than-additive effects for PH (Supplementary Figure S8). Large or

⁵³⁵ moderate effect negative epistasis is expected across subgenomes in allopolyploids, but it is

⁵³⁶ unclear why this was also observed for the Within marker set for TW.

26

5.5 Homeologous model fit

Comparing variance component estimates across different unstructured covariance matrices can be misleading as variance components can be scaled by pulling a constant out of the covariance matrix. Additionally, variance partitioning is only reliable when the covariance matrices are truly independent (Vitezica *et al.*, 2017; Huang and Mackay, 2016; Jiang *et al.*, 2017). Therefore, we do not make an attempt to discern meaning from the variance components *per se*, and instead focus the discussion on model fit diagnostics, as well as prediction accuracy from cross validation to determine the value of the predictive information included in the model.

All epistatic models using the $\{-1, 1\}$ marker parameterization provided a superior fit to the additive only model based on Akaike's Information Criterion (AIC) for all traits (Supplementary Table S4). These results were confirmed by a likelihood ratio test to determine if the epistatic variance component was zero for all traits. With the exception of the GY trait, all of the epistatic models using the $\{0, 1\}$ marker parameterization also had non-zero variance components (Supplementary Table S5), but did not result in a better fit for any models or traits. The LAVHAE method outperformed all other marker orientation schemes (Supplementary Tables S6,S7, S8 and S9). The Pairwise, Within and Across epistatic models outperformed the Homeo marker interaction set for all traits. This may be due to poor assignment of homeologous sets, or relatively fewer identifiable interactions and is discussed later.

5.6 Genomic prediction

All epistatic models resulted in higher prediction accuracies for all traits other than GY, where only marginal increases were seen for certain marker interaction sets and parameterizations (Table 4). The $\{-1, 1\}$ marker coding resulted in higher prediction accuracies with a mean increase of 0.045 over the $\{0, 1\}$ coding, and ranged from 0.007 to 0.084 higher accuracy. This increase may be due to choosing the wrong orientation using the $\{0, 1\}$

27

563 marker coding effects. While these two codings are equivalent for prediction when marker

564 effects are fixed, this is not the case for the mixed model genomic prediction environment

565 (Martini *et al.*, 2017, 2018). The discrepancy lies in shrinkage of interaction effects, where

566 the $\{0, 1\}$ marker coding should result in greater shrinkage than the $\{-1, 1\}$ marker cod-

567 ing. This can be seen from a simple example with one observation of each genotypic class

568 in $\{bbcc, bbCC, BBcc, BBCC\}$. The $\{-1, 1\}$ coding would have an interaction predictor of

569 $\{1, -1, -1, 1\}$, whereas the $\{0, 1\}$ coding would have an interaction predictor of $\{0, 0, 0, 1\}$.

570 This results in different numbers of observations per interaction class, with the $\{0, 1\}$ coding

571 contrasting 3 and 1, verses 2 and 2 for the $\{-1, 1\}$ coding. Therefore the shrinkage of the

572 $\{0, 1\}$ coding should be greater than for the $\{-1, 1\}$ coding. Martini *et al.* (2017), also noted

573 that the $\{-1, 1\}$ marker coding has a 50% chance of choosing the wrong marker orientation

574 if chosen at random, whereas the $\{0, 1\}$ marker coding has a 75% chance of being the wrong

575 marker orientation.

576   The LAVHAE marker orientation scheme was superior for prediction of all traits and

577 marker sets for the $\{-1, 1\}$ coding, but had little effect on the $\{0, 1\}$ marker coding (Sup-

578 plemental Tables S12, S13 and S14). This suggests that information can be gained from

579 orienting markers relative to one another, however, it is still unlcear what strategy should be

580 used to orient pairs of markers. In this report, marker additive effects were forced to be either

581 all positive or all negative to model the homeologous subfunctionalization hypothesis, but

582 there may be more biologically relevant orientations not explored here. Martini *et al.* (2017)

583 used a categorical interaction that included a predictor for each pairwise genotype. That

584 model was shown to be less predictive than the $\{-1, 1\}$ multiplicative model, perhaps due

585 to more linearly dependent predictors assumed to have non-zero effects. Feature selection

586 may be useful for selecting the most informative interactions from this population of linearly

587 dependent predictors. How an optimal set of orientations might be obtained without losing

588 biological meaning of the orientation warrants further investigation.

589   The proportion of non-additive genetic signal attributable to homeologous gene interac-

28

Table 4: Prediction accuracies of whole genome Additive and Pairwise epistasis, along with the Homeo, Within and Across genome marker sets for both $\{-1, 1\}$ and $\{0, 1\}$ marker coding using the LAVHAE marker orientation.

LAVHAE	Additive	Pairwise	Homeo_{-11}	Homeo_{01}	Within_{-11}	Within_{01}	Across_{-11}	Across_{01}
GY	0.601^a	0.604	$0.606\ (167\%)^b$	0.599 (-67%)	0.627 (867%)	0.600 (-33%)	0.630 (967%)	0.604 (100%)
PH	0.559	0.637	0.606 (60%)	0.580 (27%)	0.652 (119%)	0.570 (14%)	0.650 (117%)	0.584 (32%)
TW	0.515	0.576	0.560 (74%)	0.516 (2%)	0.596 (133%)	0.514 (-2%)	0.581 (108%)	0.525 (16%)
HD	0.664	0.712	0.692 (58%)	0.682 (38%)	0.710 (96%)	0.674 (21%)	0.722 (121%)	0.682 (38%)

[a]Mean Pearson correlation between predicted and observed genetic values across 10 random 5-fold cross-validation replications.

[b]The percentage of the non additive genetic predictability as relative to the the Pairwise model is shown in parentheses (equation 4).

590 tion was determined by taking the ratio of the percent increase in prediction accuracy of the

591 Homeo, Within or Across prediction models from the additive model to the increase in pre-

592 diction accuracy due to all pairwise interactions (equation 4). All three marker sets resulted

593 in higher genomic prediction accuracy than the additive only GBLUP model (G) when the

594 $\{-1, 1\}$ marker coding was used. The homeologous marker interaction set explained between

595 58% and 167% of the additional genetic signal from the additive model. This result sup-

596 ports the idea that homeologous interactions are an important feature in the wheat genome.

597 Conversely, Within and Across epistatic marker sets always resulted in a higher increase

598 in genomic prediction accuracy relative to the Homeo marker set for all traits. This may

599 suggest that the homeologous marker interactions are the least important relative to other

600 epistatic interactions within and across the subgenomes, but could also be due to the paucity

601 of these interactions relative to all possible two-way interactions, as previously discussed.

602 Another explanation might be provided by the relatively higher degree of LD across

603 Homeo marker sets than found for the Within or Across marker sets. Homeologous marker

604 sets were selected next to one another along syntenic regions of homeologous chromosome,

605 and more often shared two of the three homeoallelic markers (Supplemental Figures S13 and

606 S14). The Within and Across sets appear to have sampled the entire genome better than

607 selecting only homeologous loci, as they track more unique pairs of genomic regions. Two

608 additional samples of each Within and Across sets were showed very similar outcomes to the

609 samples shown here (see Supplementary Tables S10, S11 and S15).

610 5.7 Homeologous LD

611 The superiority of the Within and Across genomic prediction models to the Homeo genomic

612 prediction model may indicate that homeologous interactions are relatively less important

613 than other sets of interacting loci. However, homeologous marker sets had a much higher

614 tendency to be co-inherited together, as seen by relatively higher standardized LD values, D'

615 (Lewontin, 1964), than observed for either Within (KS test p-value $= 1.1 \times 10^{-6}$) or Across

30

(KS test p-value $= 2.3 \times 10^{-13}$) marker sets (Figure 6). The greater fixation of allele pairs at homeologous regions may explain the lack of increased prediction accuracy of the Homeo marker set, but this may not diminish the importance of homeologous interactions. As sets of interactions are fixed within the population, the epistatic variance becomes additive (Hill *et al.*, 2008). The higher degree of LD, *per se*, may indicate the importance of homeologous interactions.

The Green Revolution dwarfing genes are an excellent example of how pairs of homeoalleles may become fixed, or develop a tendency for co-inheritance under selection. In this example, the desirable phenotype is a semi-dwarf, due to its resistance to lodging. Therefore, wildtype *Rht-1B* alleles will usually be paired with a GA-insensitive *Rht-1D* dwarfing allele, while wildtype *Rht-1D* alleles will usually be found with a GA-insensitive *Rht-1B* dwarfing allele to confer the desirable semi-dwarf phenotype. The 'perfect' *Rht-1* markers had a large standardized D' value of 0.89, indicating that pairs of alleles were being fixed in the population.

We recognize that it is also possible that the higher degree of LD observed between homeologous marker pairs could be due to misalignment of markers to the wrong subgenome. Markers assigned to the wrong homeolog would appear in high LD simply because they are physically located near their assigned homeologous partner on the same chromosome. We used strict filtering parameters to reduce the likelihood of misalignment. This included a threshold on observed heterozygosity in the population, which could indicate alignment to more than one subgenome.

6 Further considerations

Wagner (2005) suggested that there are two potential drivers of less-than-additive (Eshed and Zamir, 1996) or synergistic (Segre *et al.*, 2005) epistasis. These drivers are i) functional redundancy, as might be expected across homeologous loci, and ii) distributed robustness of

⁶⁴¹ function, in which there can be are many pathways that can acheive the same outcome. Our

⁶⁴² observation that most epistasis is not due to homeologous interactions is supported by the

⁶⁴³ findings of Jannink *et al.* (2009), who found the synergistic epistasis signal in a wheat dataset

⁶⁴⁴ to be indicative of Wagner's distributed hypothesis, and not of the redundancy hypothesis.

⁶⁴⁵   It may be that there are few differences in protein function or expression across the three

⁶⁴⁶ subgenomes, although this seems unlikely given mounting evidence that homeologous copies

⁶⁴⁷ are differentially expressed in time, tissue and environment (Adams *et al.*, 2003; Liu and

⁶⁴⁸ Adams, 2007; Liu *et al.*, 2011; Chaudhary *et al.*, 2009; Pfeifer *et al.*, 2014; Liu *et al.*, 2015;

⁶⁴⁹ Zhang *et al.*, 2016; Mutti *et al.*, 2017). We were unable to assign homeologous pairs to

⁶⁵⁰ all genes within the genome, suggesting that many of these potential sites for interacting

⁶⁵¹ loci were lost during polyploidization. Rapid loss of genetic material due to genome shock

⁶⁵² (McClintock, 1984) is common in newly synthesized allopolyploids (Comai *et al.*, 2003; Chen

⁶⁵³ and Ni, 2006), as has been shown in synthetic allopolyploid wheat (Ozkan *et al.*, 2001;

⁶⁵⁴ Kashkush *et al.*, 2002). Other interacting loci may have undergone epigenetic (Comai, 2000;

⁶⁵⁵ Lee and Chen, 2001; Comai *et al.*, 2003) or transposon induced silencing of one or more

⁶⁵⁶ homeoalleles (Kashkush *et al.*, 2003; Wang *et al.*, 2004).

⁶⁵⁷   The large portions of duplicated genes retainment across subgenomes suggests there is a

⁶⁵⁸ benefit to their maintenance. Duplicate copies may be important contributors to differential

⁶⁵⁹ genotype performance in contrasting environments. Unfortunately, the CNLM dataset lacks

⁶⁶⁰ sufficient genotype by environment variation to properly ask this question (data not shown).

⁶⁶¹ Experiments designed to explicitly model the phenotypic effect of differential homeologous

⁶⁶² gene expression across contrasting environments will be necessary to provide a satisfactory

⁶⁶³ answer.

⁶⁶⁴   One of the challenges of using diverse panels of individuals is that marker proximity to

⁶⁶⁵ a functional mutation is not necessarily indicative of high LD between the two sites. Sig-

⁶⁶⁶ nificantly older or newer marker mutations may be in weak LD with a functional mutation

⁶⁶⁷ despite close physical proximity, at least until a genetic bottleneck brings them back into

32

high LD, such as in a bi-parental population (Flint-Garcia *et al.*, 2003; Weir, 2008). Other strategies to determine functional homeologous regions relax which sets of markers are considered homeologous. This has been accomplished by allowing pairwise relationships with all markers across entire subgenomes (Santantonio *et al.*, 2018b) or on syntenic chromosome arms (Santantonio *et al.*, 2018a), with mixed success. The construction of smaller haplotypes in a manner similar to Gao *et al.* (2017) may also improve functional pairing of homeologous alleles. Higher depth sequencing and advances in marker imputation may also aid in detection of homeologous epistasis.

The TILLING population developed by Krasileva *et al.* (2017) could be a useful resource for future investigation into homeoallelic gene interactions. Lines with complementary loss of function homeologous genes could be used to develop bi-parental mapping populations to test the degree of subfunctionalization with the high statistical power afforded by allele frequencies of 0.5. So called 'synthetic' wheat populations formed by crossing common wheat with newly synthesized allohexaploids containing durum A and B genomes coupled to an *Ae. taushii* D genome (Sorrells *et al.*, 2011, e.g.), and may prove powerful for detection of interactions between the common wheat homeologs and their durum and *Ae. taushii* ancestors.

7   Conclusion

While much epistasis is partitioned to additive variance, it has been shown to be prevalent (Forsberg *et al.*, 2017), and is important for maintaining long term selection (Carlborg *et al.*, 2006; Paixão and Barton, 2016). Our results indicate that homeologous interactions contribute to the total genetic variance of the CNLM population. However, sampling interactions across non-syntenic regions was superior for all traits examined, suggesting that homeologous epistasis make up a minority of the non-additive genetic variance. The biological state of allopolyploids, along with the suggestive evidence presented here, demonstrate
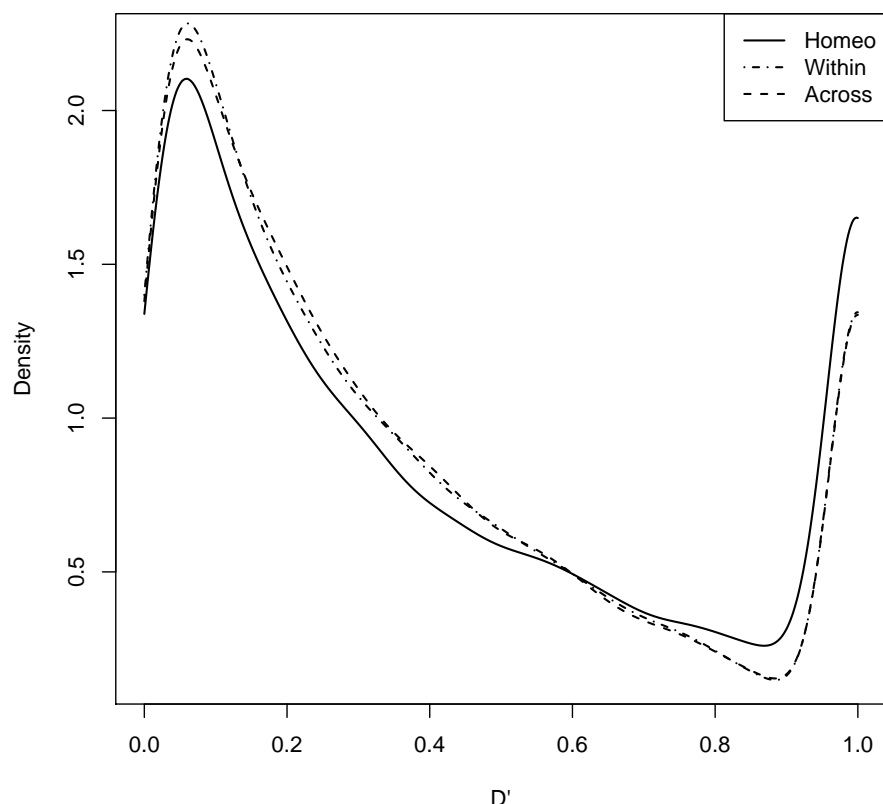
33

Figure 6: Smoothed densities of standardized D' statistics of linkage disequilibrium for expected and observed joint allele frequencies for Homeo, Within and Across marker sets. Kolmogorov-Smirnov (KS) tests were used to determine if the distribution of LD differed between Homeo and Within (KS p-value = 1.1×10^{-6}) or Across (KS p-value = 2.3×10^{-13}) marker sets.

693   that there is value in further investigation of homeologous interactions.

694   The most important trait, GY, showed little to no evidence of homeologous subfunction-

695   alization. This may be due to the highly polygenic nature of the trait, where essentially

696   all functional genetic differences in the population should contribute to GY. Modern plant

697   breeding has likely driven large effect homeologous allele pair interactions to fixation in elite

698   wheat genotypes. The implementation of the semi-dwarf phenotype provides perhaps the

699   most important example where fixation of specific pairs of homeoalleles resulted in the single

700   largest increase in wheat grain production in modern agriculture.

34

Prediction of unobserved homeologous allele pairs may prove difficult, as it currently is in diploid hybrids. However, large populations may be use to identify beneficial homeologous combinations that may subsequently be used for selection of unobserved lines before intensive field trials are conducted.

Treating the genome as consisting of purely additive gene action assumes that genes are independent machines, whose products sum to the final value of an individual. While convenient for selection, this is almost certainly not true when we consider the molecular mechanisms of biological organisms. Instead, genes work in concert to produce an observable phenotype. To this day, breeders of allopolyploid crops have treated allopolyploids as diploids for simplicity, but we now have the technical ability to view and start to breed these organisms as the ancient immortal hybrids that they are.

8   Acknowledgments

35

726 who were vital in implementing, collecting and processing the materials used to build the

727 CNLM dataset.

References

729 Adams, K. L., R. Cronn, R. Percifield, and J. F. Wendel, 2003 Genes duplicated by polyploidy

730 show unequal contributions to the transcriptome and organ-specific reciprocal silencing.

731 Proceedings of the National Academy of sciences **100**: 4649–4654.

732 Adams, K. L. and J. F. Wendel, 2005 Polyploidy and genome evolution in plants. Current

733 opinion in plant biology **8**: 135–141.

734 Akhunova, A. R., R. T. Matniyazov, H. Liang, and E. D. Akhunov, 2010 Homoeolog-specific

735 transcriptional bias in allopolyploid wheat. BMC genomics **11**: 505.

736 Allan, R. and O. Vogel, 1965 Monosomic analysis of red seed color in wheat 1. Crop Science

737 **5**: 474–475.

738 Allan, R., O. Vogel, and J. Craddock, 1959 Comparative response to gibberellic acid of dwarf,

739 semidwarf, and standard short and tall winter wheat varieties 1. Agronomy Journal **51**:

740 737–740.

741 Allard, R. W. and A. Bradshaw, 1964 Implications of genotype-environmental interactions

742 in applied plant breeding. Crop science **4**: 503–508.

743 Álvarez-Castro, J. M. and Ö. Carlborg, 2007 A unified model for functional and statistical

744 epistasis and its application in quantitative trait loci analysis. Genetics **176**: 1151–1167.

745 Assis, R. and D. Bachtrog, 2013 Neofunctionalization of young duplicate genes in drosophila.

746 Proceedings of the National Academy of Sciences **110**: 17409–17414.

747 Bingham, E., R. Groose, D. Woodfield, and K. Kidwell, 1994 Complementary gene interac-

748 tions in alfalfa are greater in autotetraploids than diploids. Crop Science **34**: 823–829.

36

Birchler, J. A., H. Yao, S. Chudalayandi, D. Vaiman, and R. A. Veitia, 2010 Heterosis. The Plant Cell **22**: 2105–2112.

Blanc, G. and K. H. Wolfe, 2004 Functional divergence of duplicated genes formed by polyploidy during arabidopsis evolution. The Plant Cell **16**: 1679–1691.

Börner, A., J. Plaschke, V. Korzun, and A. Worland, 1996 The relationships between the dwarfing genes of wheat and rye. Euphytica **89**: 69–75.

Butler, D., 2009 *asreml: asreml() fits the linear mixed model*. R package version 3.0.

Camacho, C., G. Coulouris, V. Avagyan, N. Ma, J. Papadopoulos, *et al.*, 2009 Blast+: architecture and applications. BMC bioinformatics **10**: 421.

Carlborg, Ö., L. Jacobsson, P. Åhgren, P. Siegel, and L. Andersson, 2006 Epistasis and the release of genetic variation during long-term selection. Nature genetics **38**: 418.

Chaudhary, B., L. Flagel, R. M. Stupar, J. A. Udall, N. Verma, *et al.*, 2009 Reciprocal silencing, transcriptional bias and functional divergence of homeologs in polyploid cotton (gossypium). Genetics **182**: 503–517.

Chen, Z. J., 2010 Molecular mechanisms of polyploidy and hybrid vigor. Trends in plant science **15**: 57–71.

Chen, Z. J., 2013 Genomic and epigenetic insights into the molecular bases of heterosis. Nature Reviews Genetics **14**: 471.

Chen, Z. J. and Z. Ni, 2006 Mechanisms of genomic rearrangements and gene expression changes in plant polyploids. Bioessays **28**: 240–252.

Comai, L., 2000 Genetic and epigenetic interactions in allopolyploid plants. Plant molecular biology **43**: 387–399.

771 Comai, L., A. Madlung, C. Josefsson, and A. Tyagi, 2003 Do the different parental heteromes
772   cause genomic shock in newly formed allopolyploids? Philosophical Transactions of the
773   Royal Society of London B: Biological Sciences **358**: 1149–1155.

774 Dahl, D. B., 2016 *xtable: Export Tables to LaTeX or HTML*. R package version 1.8-2.

775 Devos, K., J. Dubcovsky, J. Dvořák, C. Chinoy, and M. Gale, 1995 Structural evolution
776   of wheat chromosomes 4a, 5a, and 7b and its impact on recombination. Theoretical and
777   Applied Genetics **91**: 282–288.

778 Duarte, J. M., L. Cui, P. K. Wall, Q. Zhang, X. Zhang, *et al.*, 2005 Expression pattern
779   shifts following duplication indicative of subfunctionalization and neofunctionalization in
780   regulatory genes of arabidopsis. Molecular biology and evolution **23**: 469–478.

781 Dubcovsky, J. and J. Dvořák, 2007 Genome plasticity a key factor in the success of polyploid
782   wheat under domestication. Science **316**: 1862–1866.

783 Ellis, M., W. Spielmeyer, K. Gale, G. Rebetzke, and R. Richards, 2002 ” perfect” markers
784   for the rht-b1b and rht-d1b dwarfing genes in wheat. Theoretical and Applied Genetics
785   **105**: 1038–1042.

786 Ellstrand, N. C. and K. A. Schierenbeck, 2000 Hybridization as a stimulus for the evolution
787   of invasiveness in plants? Proceedings of the National Academy of Sciences **97**: 7043–7050.

788 Eshed, Y. and D. Zamir, 1996 Less-than-additive epistatic interactions of quantitative trait
789   loci in tomato. Genetics **143**: 1807–1817.

790 Feldman, M. and A. A. Levy, 2012 Genome evolution due to allopolyploidization in wheat.
791   Genetics **192**: 763–774.

792 Feldman, M., A. A. Levy, T. Fahima, and A. Korol, 2012 Genomic asymmetry in allopoly-
793   ploid plants: wheat as a model. Journal of experimental botany **63**: 5045–5059.

794 Flint-Garcia, S. A., J. M. Thornsberry, and E. S. Buckler IV, 2003 Structure of linkage
795   disequilibrium in plants. Annual review of plant biology **54**: 357–374.

796 Force, A., M. Lynch, F. B. Pickett, A. Amores, Y.-l. Yan, *et al.*, 1999 Preservation of
797   duplicate genes by complementary, degenerative mutations. Genetics **151**: 1531–1545.

798 Forsberg, S. K., J. S. Bloom, M. J. Sadhu, L. Kruglyak, and Ö. Carlborg, 2017 Accounting
799   for genetic interactions improves modeling of individual quantitative trait phenotypes in
800   yeast. Nature genetics **49**: 497.

801 Gale, M. and G. A. Marshall, 1976 The chromosomal location of gai 1 and rht 1, genes for
802   gibberellin insensitivity and semi-dwarfism, in a derivative of norin 10 wheat. Heredity **37**:
803   283.

804 Gale, M. D., C. Law, and A. Worland, 1975 The chromosomal location of a major dwarfing
805   gene from norin 10 in new british semi-dwarf wheats. Heredity **35**: 417.

806 Gao, N., J. W. Martini, Z. Zhang, X. Yuan, H. Zhang, *et al.*, 2017 Incorporating gene
807   annotation into genomic predictionof complex phenotypes. Genetics pp. genetics–300198.

808 Gault, C. M., K. A. Kremling, and E. S. Buckler, 2018 Tripsacum de novo transcriptome
809   assemblies reveal parallel gene evolution with maize after ancient polyploidy. The Plant
810   Genome .

811 Gilmour, A., 1997 Asreml for testing fixed effects and estimating multiple trait variance
812   components. In *Proceedings of the Association for the Advancement of Animal Breeding*
813   *and Genetics*, volume 12, pp. 386–390.

814 Gu, Z., L. Gu, R. Eils, M. Schlesner, and B. Brors, 2014 circlize implements and enhances
815   circular visualization in r. Bioinformatics **30**: 2811–2812.

816 Haldane, J., 1933 The part played by recurrent mutation in evolution. American Naturalist
817   pp. 5–19.

818 He, D., Z. Wang, and L. Parida, 2015 Data-driven encoding for quantitative genetic trait
819   prediction. In *BMC bioinformatics*, volume 16, p. S10, BioMed Central Ltd.

820 Herskowitz, I., 1987 Functional inactivation of genes by dominant negative mutations. Nature
821   **329**: 219–222.

822 Hill, W. G., M. E. Goddard, and P. M. Visscher, 2008 Data and theory point to mainly
823   additive genetic variance for complex traits. PLoS Genet **4**: e1000008.

824 Huang, W. and T. F. Mackay, 2016 The genetic architecture of quantitative traits cannot
825   be inferred from variance component analysis. PLoS genetics **12**: e1006421.

826 IWGSC, I. W. G. S. C., 2018, accepted Shifting the limits in wheat research and breeding
827   using a fully annotated reference genome by the international wheat genome sequencing
828   consortium (iwgsc). Science .

829 Jannink, J.-L., L. Moreau, G. Charmet, and A. Charcosset, 2009 Overview of qtl detection
830   in plants and tests for synergistic epistatic interactions. Genetica **136**: 225.

831 Jiang, Y. and J. C. Reif, 2015 Modeling epistasis in genomic selection. Genetics **201**: 759–
832   768.

833 Jiang, Y., R. H. Schmidt, Y. Zhao, and J. C. Reif, 2017 A quantitative genetic framework
834   highlights the role of epistatic effects for grain-yield heterosis in bread wheat. Nature
835   genetics **49**: 1741.

836 Kashkush, K., M. Feldman, and A. A. Levy, 2002 Gene loss, silencing and activation in a
837   newly synthesized wheat allotetraploid. Genetics **160**: 1651–1659.

838 Kashkush, K., M. Feldman, and A. A. Levy, 2003 Transcriptional activation of retrotrans-
839   posons alters the expression of adjacent genes in wheat. Nature genetics **33**: 102.

840 Krasileva, K. V., H. A. Vasquez-Gross, T. Howell, P. Bailey, F. Paraiso, *et al.*, 2017 Uncover-
841   ing hidden variation in polyploid wheat. Proceedings of the National Academy of Sciences
842   **114**: E913–E921.

843 Law, C., J. Sutka, and A. Worland, 1978 A genetic study of day-length response in wheat.
844   Heredity **41**: 185.

845 Lee, H.-S. and Z. J. Chen, 2001 Protein-coding genes are epigenetically regulated in ara-
846   bidopsis polyploids. Proceedings of the National Academy of Sciences **98**: 6753–6758.

847 Lewontin, R., 1964 The interaction of selection and linkage. i. general considerations; het-
848   erotic models. Genetics **49**: 49–67.

849 Liu, S.-L., G. J. Baute, and K. L. Adams, 2011 Organ and cell type–specific complemen-
850   tary expression patterns and regulatory neofunctionalization between duplicated genes in
851   arabidopsis thaliana. Genome biology and evolution **3**: 1419–1436.

852 Liu, Z. and K. L. Adams, 2007 Expression partitioning between genes duplicated by poly-
853   ploidy under abiotic stress and during organ development. Current Biology **17**: 1669–1674.

854 Liu, Z., M. Xin, J. Qin, H. Peng, Z. Ni, *et al.*, 2015 Temporal transcriptome profiling reveals
855   expression partitioning of homeologous genes contributing to heat and drought acclimation
856   in wheat (triticum aestivum l.). BMC plant biology **15**: 152.

857 Lynch, M. and J. S. Conery, 2000 The evolutionary fate and consequences of duplicate genes.
858   Science **290**: 1151–1155.

859 Lynch, M. and A. Force, 2000 The probability of duplicate gene preservation by subfunc-
860   tionalization. Genetics **154**: 459–473.

861 Mac Key, J., 1970 Significance of mating systems for chromosomes and gametes in polyploids.
862   Hereditas **66**: 165–176.

863 Marcussen, T., S. R. Sandve, L. Heier, M. Spannagl, M. Pfeifer, *et al.*, 2014 Ancient hy-
864   bridizations among the ancestral genomes of bread wheat. Science **345**: 1250092.

865 Martini, J. W., N. Gao, D. F. Cardoso, V. Wimmer, M. Erbe, *et al.*, 2017 Genomic prediction
866   with epistasis models: on the marker-coding-dependent performance of the extended gblup
867   and properties of the categorical epistasis model (ce). BMC bioinformatics **18**: 3.

868 Martini, J. W., F. Rosales, N.-T. Ha, T. Kneib, J. Heise, *et al.*, 2018 Lost in translation:
869   On the impact of data coding on penalized regression with interactions. arXiv preprint
870   arXiv:1806.03729 .

871 Martini, J. W., V. Wimmer, M. Erbe, and H. Simianer, 2016 Epistasis and covariance: how
872   gene interaction translates into genomic relationship. Theoretical and Applied Genetics
873   **129**: 963–976.

874 McClintock, B., 1984 The significance of responses of the genome to challenge. Science **266**:
875   792–801.

876 McVittie, J. A., M. D. Gale, G. A. Marshall, and B. Westcott, 1978 The intra-chromosomal
877   mapping of the norin 10 and tom thumb dwarfing genes. Heredity **40**: 67.

878 Metzger, R. and B. Silbaugh, 1970 Location of genes for seed coat color in hexaploid wheat,
879   triticum aestivum l. 1. Crop science **10**: 495–496.

880 Microsoft, R. C. T., 2017 *Microsoft R Open*. Microsoft, Redmond, Washington.

881 Mutti, J. S., R. K. Bhullar, and K. S. Gill, 2017 Evolution of gene expression balance among
882   homeologs of natural polyploids. G3: Genes, Genomes, Genetics **7**: 1225–1237.

883 Nagasaki, H., M. Arita, T. Nishizawa, M. Suwa, and O. Gotoh, 2005 Species-specific variation
884   of alternative splicing and transcriptional initiation in six eukaryotes. Gene **364**: 53–62.

885 Ohno, S., 1970 *Evolution by Gene Duplication*. Springer, New York.

Ohta, T., 1987 Simulating evolution by gene duplication. Genetics **115**: 207–213.

Osborn, T. C., J. C. Pires, J. A. Birchler, D. L. Auger, Z. J. Chen, *et al.*, 2003 Understanding mechanisms of novel gene expression in polyploids. Trends in genetics **19**: 141–147.

Ozkan, H., A. A. Levy, and M. Feldman, 2001 Allopolyploidy-induced rapid genome evolution in the wheat (aegilops–triticum) group. The Plant Cell **13**: 1735–1747.

Paixão, T. and N. H. Barton, 2016 The effect of gene interactions on the long-term response to selection. Proceedings of the National Academy of Sciences **113**: 4422–4427.

Pfeifer, M., K. G. Kugler, S. R. Sandve, B. Zhan, H. Rudi, *et al.*, 2014 Genome interplay in the grain transcriptome of hexaploid bread wheat. Science **345**: 1250091.

Poland, J., 2018 personal communication.

Pumphrey, M., J. Bai, D. Laudencia-Chingcuanco, O. Anderson, and B. S. Gill, 2009 Nonadditive expression of homoeologous genes is established upon polyploidization in hexaploid wheat. Genetics **181**: 1147–1157.

R Core Team, 2015 *R: A Language and Environment for Statistical Computing*. R Foundation for Statistical Computing, Vienna, Austria.

Rastogi, S. and D. A. Liberles, 2005 Subfunctionalization of duplicated genes as a transition state to neofunctionalization. BMC evolutionary biology **5**: 28.

Santantonio, N., J.-L. Jannink, and M. E. Sorrells, 2018a A low resolution epistasis mapping approach to identify chromosome arm interactions in allohexaploid wheat. bioRxiv p. 377713.

Santantonio, N., J.-L. Jannink, and M. E. Sorrells, 2018b Prediction of subgenome additive and interaction effects in allohexaploid wheat. bioRxiv p. 373605.

908 Scarth, R. and C. Law, 1983 The location of the photoperiod gene, ppd2 and an additional
909   genetic factor for ear-emergence time on chromosome 2b of wheat. Heredity **51**: 607.

910 Segovia-Lerma, A., L. Murray, M. Townsend, and I. Ray, 2004 Population-based diallel
911   analyses among nine historically recognized alfalfa germplasms. Theoretical and applied
912   genetics **109**: 1568–1575.

913 Segre, D., A. DeLuna, G. M. Church, and R. Kishony, 2005 Modular epistasis in yeast
914   metabolism. Nature genetics **37**: 77.

915 Soltis, D. E., V. A. Albert, J. Leebens-Mack, C. D. Bell, A. H. Paterson, *et al.*, 2009
916   Polyploidy and angiosperm diversification. American journal of botany **96**: 336–348.

917 Soltis, P. S. and D. E. Soltis, 2009 The role of hybridization in plant speciation. Annual
918   review of plant biology **60**: 561–588.

919 Sorrells, M. E., J. P. Gustafson, D. Somers, S. Chao, D. Benscher, *et al.*, 2011 Reconstruction
920   of the synthetic w7984× opata m85 wheat reference population. Genome **54**: 875–882.

921 Stoltzfus, A., 1999 On the possibility of constructive neutral evolution. Journal of Molecular
922   Evolution **49**: 169–181.

923 Tantau, T., 2018 *The TikZ and PGF Packages*.

924 te Beest, M., J. J. Le Roux, D. M. Richardson, A. K. Brysting, J. Suda, *et al.*, 2011 The
925   more the better? the role of polyploidy in facilitating plant invasions. Annals of botany
926   **109**: 19–45.

927 VanRaden, P., 2008 Efficient methods to compute genomic predictions. Journal of dairy
928   science **91**: 4414–4423.

929 Veitia, R. A., 2007 Exploring the molecular etiology of dominant-negative mutations. The
930   Plant Cell **19**: 3843–3851.

Vitezica, Z. G., A. Legarra, M. A. Toro, and L. Varona, 2017 Orthogonal estimates of variances for additive, dominance, and epistatic effects in populations. Genetics **206**: 1297–1307.

Wagner, A., 2005 Distributed robustness versus redundancy as causes of mutational robustness. Bioessays **27**: 176–188.

Walsh, J. B., 1995 How often do duplicated genes evolve new functions? Genetics **139**: 421–428.

Wang, J., L. Tian, A. Madlung, H.-S. Lee, M. Chen, *et al.*, 2004 Stochastic and epigenetic changes of gene expression in arabidopsis polyploids. Genetics **167**: 1961–1973.

Weir, B., 2008 Linkage disequilibrium and association mapping. Annu. Rev. Genomics Hum. Genet. **9**: 129–142.

Welsh J.R., P. B., Keim D.L. and R. R.D., 1973 Genetic control of photoperiod response in wheat. In *Proceedings of the fourth International Wheat Genetics Symposium*, edited by S. E.R. and S. L.E.S., pp. 879–884, University of Missouri, Columbia, Mo.

Wendel, J. F., 2000 Genome evolution in polyploids. In *Plant molecular evolution*, pp. 225–249, Springer.

Wood, A. R., M. A. Tuke, M. A. Nalls, D. G. Hernandez, S. Bandinelli, *et al.*, 2014 Another explanation for apparent epistasis. Nature **514**: E3.

Zeng, Z.-B. and C. C. Cockerham, 1993 Mutation models and quantitative genetic variation. Genetics **133**: 729–736.

Zeng, Z.-B., T. Wang, and W. Zou, 2005 Modeling quantitative trait loci and interpretation of models. Genetics **169**: 1711–1725.

Zhang, Y., Z. Liu, A. A. Khan, Q. Lin, Y. Han, *et al.*, 2016 Expression partitioning of homeologs and tandem duplications contribute to salt tolerance in wheat (triticum aestivum l.). Scientific reports **6**: 21476.

Zhang, Z., E. Ersoz, C.-Q. Lai, R. J. Todhunter, H. K. Tiwari, *et al.*, 2010 Mixed linear model approach adapted for genome-wide association studies. Nature genetics **42**: 355–360.

A1   Appendix 1 - RIL population

The population was formed from a cross between two Cornell soft winter wheat lines, NY91017-8080 and Caledonia. Caledonia contains a GA-insensitive 4D allele, d, and a wildtype 4B allele, B, while NY91017-8080 has a GA-insensitive 4B allele, b, and the wild type 4D allele, D. The population consisting of 192 individuals was planted in single row plots in Ithaca NY and measured for plant height in 2008. The population was screened for loci influencing plant height on chromosomes 4B and 4D using genotyping by sequencing (GBS) markers. The markers with the lowest p-value on the short arms of 4B and 4D were used to indicate the *Rht-1* gene in this study. Only individuals with homozygous genotype calls for both loci were included to test for epistasis. This resulted in 19 double dwarfs ($bbdd$), 51 D genome semi-dwarfs ($BBdd$), 35 B genome semi-dwarfs($bbDD$), and 53 tall ($BBDD$), for a total of 158 individuals. It appears that the Caledonia parent plant used in the cross was heterozygous for the D genome dwarfing allele, resulting in the 1:2 segregation ratio for the $d : D$ alleles, and was confirmed by the genotype call for that plant.

A2   Appendix 2 - Coding Sequence Alignment

Alignments of coding sequences was accomplished with BLAST+, allowing up to 10 alignments with an e-value cutoff of 1e-5. Alignments were only considered if they aligned to 80% or more of the query gene. Of the 110,790 coding sequences, 13,111 triplicate sets

with one gene on each homeologous chromosome (representing 39,333 genes) were identified with no other alignments meeting the criterion. An additional 5,073 triplicates (representing 15,219 genes) were added by selecting the top 2 alignments if they were on the corresponding homeologous chromosomes. Duplicate sets were also included if there was not a third alignment to one of the three sub-genomes, adding an additional 5,612 duplicates. The coding sequences for which we did not identify homeologous genes either appeared to be singletons (24,695 coding sequences) that did not have a good alignment to a gene on a homeologous chromosome, or had many alignments across the genome making it impossible to determine with certainty which alignments were truly homeologous (20,319 coding sequences).

A3   Appendix 3 - Change of reference

Following Álvarez-Castro and Carlborg (2007), we demonstrate the change-of-reference operation simplified for inbred populations. For $\{0,1\}$ marker coding and allowing G_1 to be the reference genotype, the genotypic values at a single locus can be represented as

$$\mathbf{G} = \begin{bmatrix} G_1 \\ G_2 \end{bmatrix} = \mathbf{S}_{01}\mathbf{E}_{01} = \begin{bmatrix} 1 & 0 \\ 1 & 1 \end{bmatrix} \begin{bmatrix} \mu \\ a \end{bmatrix} \tag{5}$$

where $\mathbf{S}_{01}$ is the marker score matrix using the $\{0,1\}$ marker parameterization and $\mathbf{E}_{01}$ is the vector of expected values. For the two locus epistasis model, the four genotypic values are then

$$\mathbf{G} = \begin{bmatrix} G_{11} \\ G_{12} \\ G_{21} \\ G_{22} \end{bmatrix} = (\mathbf{S}_{01} \otimes \mathbf{S}_{01})\mathbf{E}_{01} = \begin{bmatrix} 1 & 0 & 0 & 0 \\ 1 & 0 & 1 & 0 \\ 1 & 1 & 0 & 0 \\ 1 & 1 & 1 & 1 \end{bmatrix} \begin{bmatrix} \mu \\ a_1 \\ a_2 \\ a_1a_2 \end{bmatrix} \tag{6}$$

47

992   The three locus interaction is extended by

$$\mathbf{G} = (\mathbf{S}_{01} \otimes \mathbf{S}_{01} \otimes \mathbf{S}_{01}) \left[\mu \ a_1 \ a_2 \ a_1 a_2 \ a_3 \ a_1 a_3 \ a_2 a_3 \ a_1 a_2 a_3 \right]^{\mathrm{T}} \tag{7}$$

To shift from $\{-1, 1\}$ coding estimates, $\boldsymbol{\beta}_{-11}$, to $\{0, 1\}$ coding estimates, $\boldsymbol{\beta}_{01}$ the following transformation exists (Álvarez-Castro and Carlborg, 2007). Let $\mathbf{S}_{-11}$ indicate the $\{-1, 1\}$ marker parameterization

$$\mathbf{S}_{-11} = \begin{bmatrix} 1 & -1 \\ 1 & 1 \end{bmatrix}$$

993   then $\mathbf{E}_{01} = (\mathbf{S}_{01}^{-1} \otimes \mathbf{S}_{01}^{-1})(\mathbf{S}_{-11} \otimes \mathbf{S}_{-11})\mathbf{E}_{-11}$.

994   S1   Supplementary Materials

Table S1: ANOVA table for *Rht-1B* and *Rht-1D* linked GBS markers and their epistatic interaction for plant height (cm) in 158 RIL lines derived from NY91017-8080 × Caledonia.

Source	df	SS	MS	F value	$-\log_{10}$(p-value)
SNP36427	1	7065	7065	53.5	10.9
SNP11172	1	7391	7391	56.0	11.3
SNP36427:SNP11172	1	1243	1243	9.4	2.6
Residuals	154	20323	132		

Table S2: Table of genotype frequencies for the *Rht-1* linked homeologous GBS markers in the CNLM population. The $+$ and $-$ signs indicate the wildtype and mutant alleles, respectively. The margins indicate the marker allele frequencies.

	S4D_PART1_10982050$^-$	S4D_PART1_10982050$^+$	
S4B_PART1_38624956$^-$	0.022	0.095	0.117
S4B_PART1_38624956$^+$	0.525	0.357	0.883
	0.547	0.452	$D' = 0.66$

Table S3: Table of genotype frequencies for the 'perfect' *Rht-1* markers in the CNLM population. The $+$ and $-$ signs indicate the wildtype and mutant alleles, respectively. The margins indicate the marker allele frequencies.

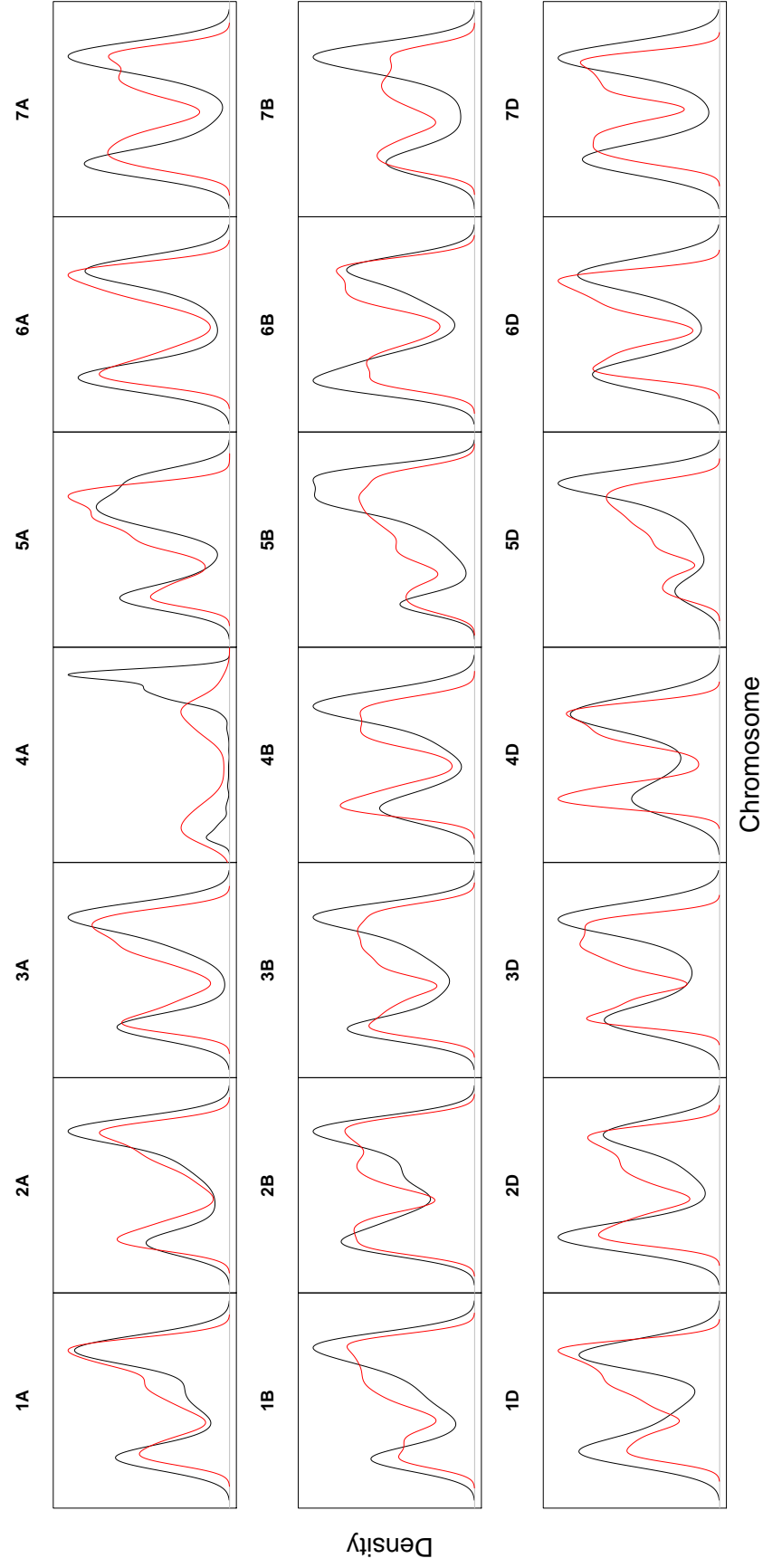|	KASP_RhtD1$^-$	KASP_RhtD1$^+$	
KASP_cimRhtB1_snp$^-$	0.008	0.093	0.101
KASP_cimRhtB1_snp$^+$	0.721	0.178	0.899
	0.729	0.271	$D' = 0.89$

Figure S1: Smoothed densities of GBS markers (black) and genes (red) along the 21 wheat chromosomes in the CNLM population.
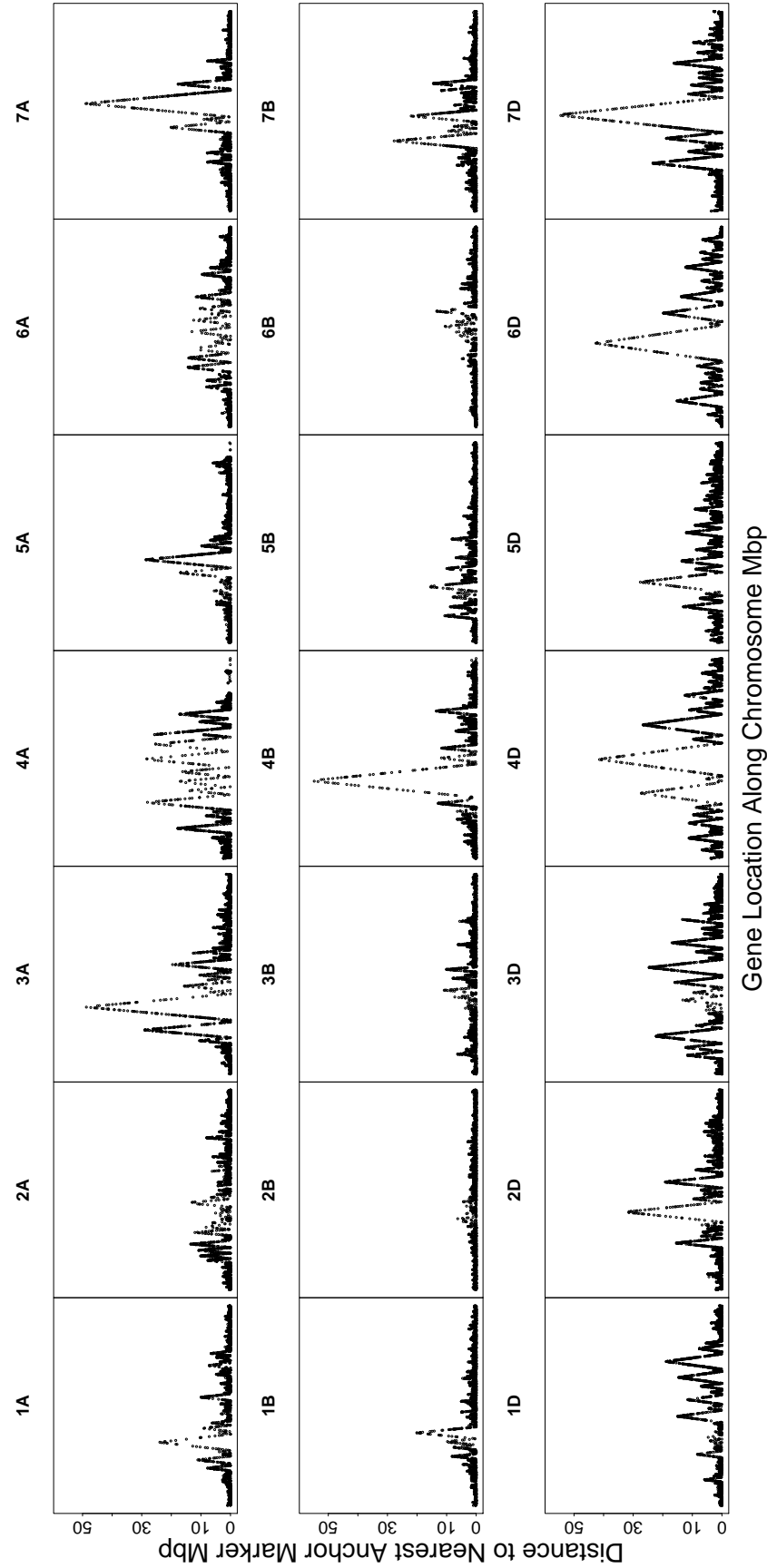
Figure S2: Distance of genes from their nearest GBS anchor marker along the 21 wheat chromosomes in the CNLM population.

Figure S3: LAVHAE oriented homeologous marker pair additive effects with point size representing the magnitude of the two-way homeologous interaction effect, and the color denoting the direction of that effect where black is positive and red is negative. Four simulated phenotypes sampled to obtain no epistatic interactions, GY, PH, TW and HD, are shown.

Figure S4: Quantile quantile plot of the ordered estimated homeologous interaction effects plotted against those from a simulated phenotype sampled to obtain no epistatic i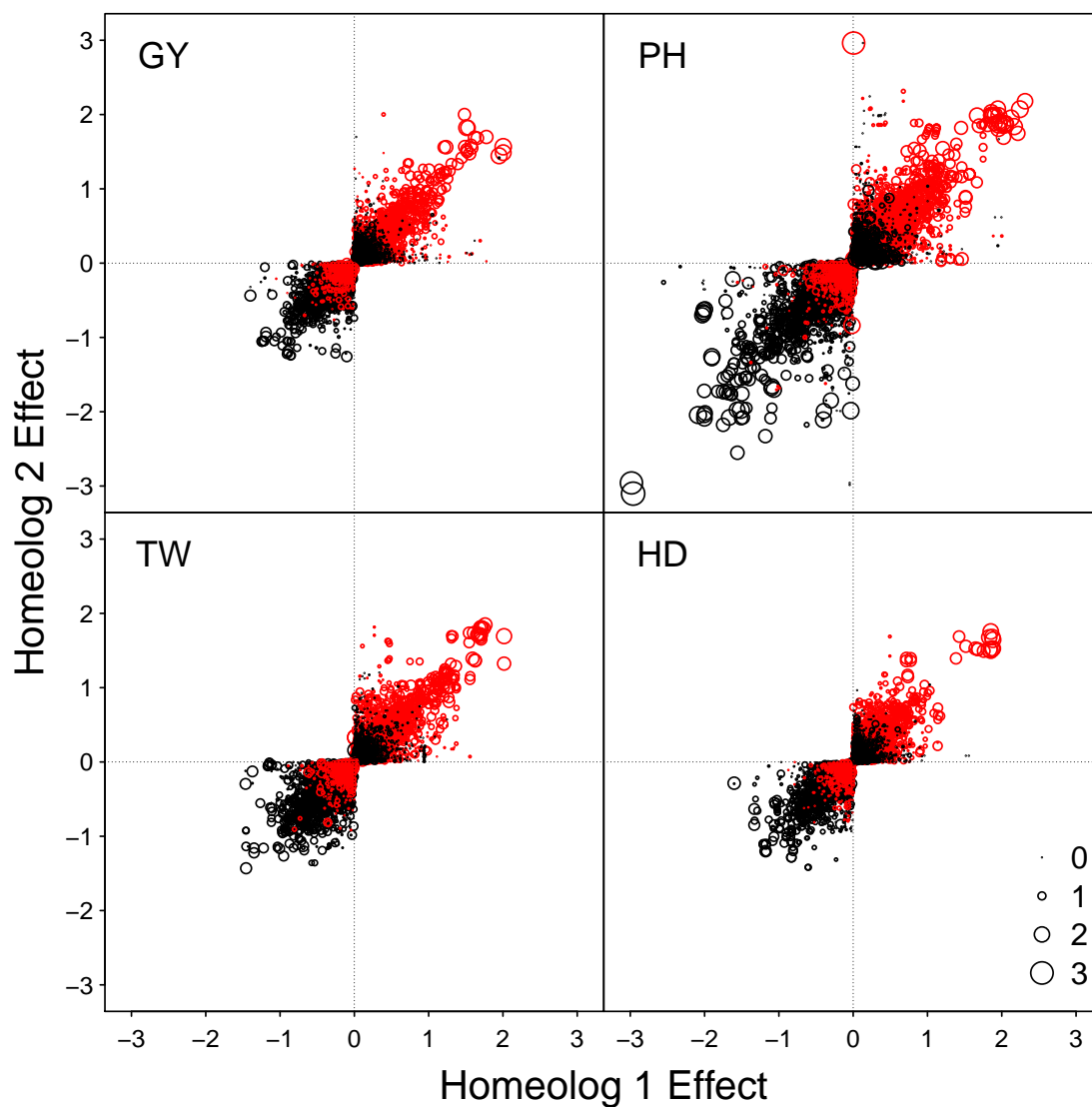nteractions using the LAVHAE marker orientation. Markers scores were permuted before simulation of the phenotype to remove LD between markers. Interaction effects have been multiplied by the effect sign of the corresponding additive effects to emphasize the relationship between the additive and interaction effects.

Figure S5: Quantile quantile plot of the ordered estimated homeologous interaction effects plotted against those from a simulated phenotype sampled to obtain no epistatic interactions using the HTEV marker orientation. Interaction effects have been multiplied by the effect sign of the corresponding additive effects to emphasize the relationship between the additive and interaction effects.
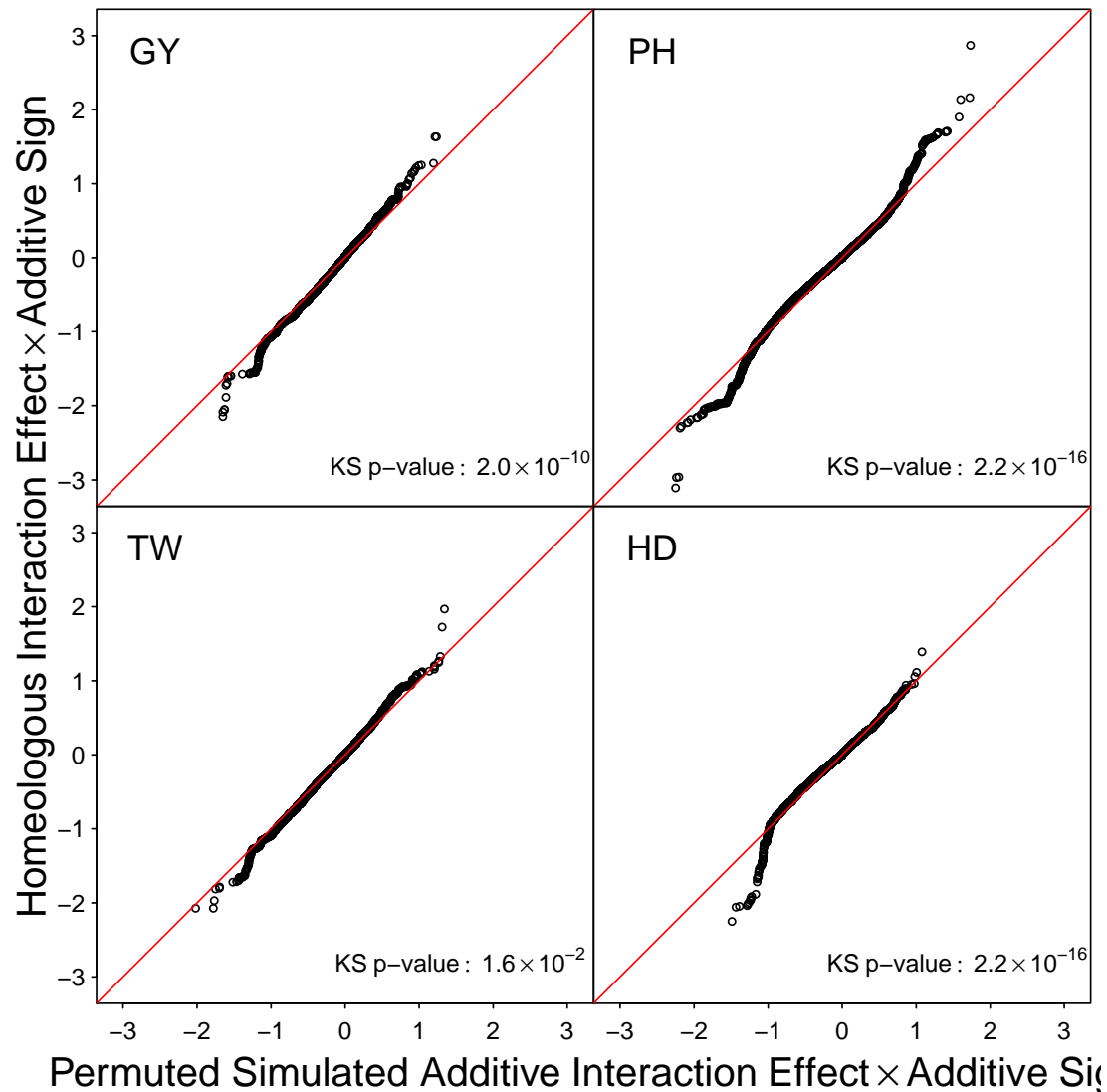
Figure S6: Quantile quantile plot of the ordered estimated homeologous interaction effects plotted against those from a simulated phenotype sampled to obtain no epistatic interactions using the HTEV marker orientation. Markers scores were permuted before simulation of the phenotype to remove LD between markers. Interaction effects have been multiplied by the effect sign of the corresponding additive effects to emphasize the relationship between the additive and interaction effects.

Figure S7: Quantile quantile plot of the ordered estimated homeologous interaction effects plotted against those from marker sets sampled within subgenome chromosomes (Within) using the LAVHAE . Interaction effects have been multiplied by the effect sign of the corresponding additive effects to emphasize the relationship between the additive and interaction effects.
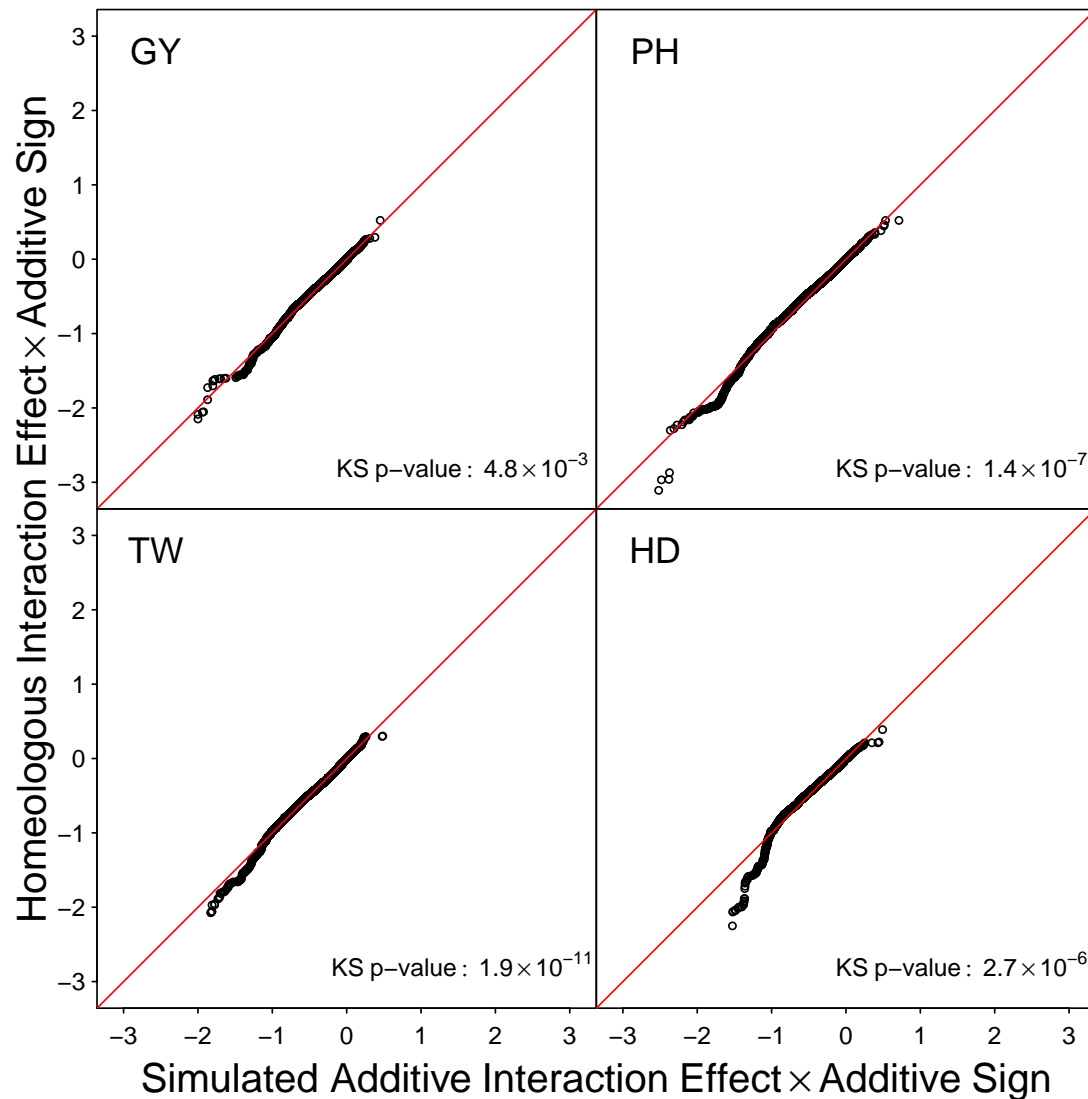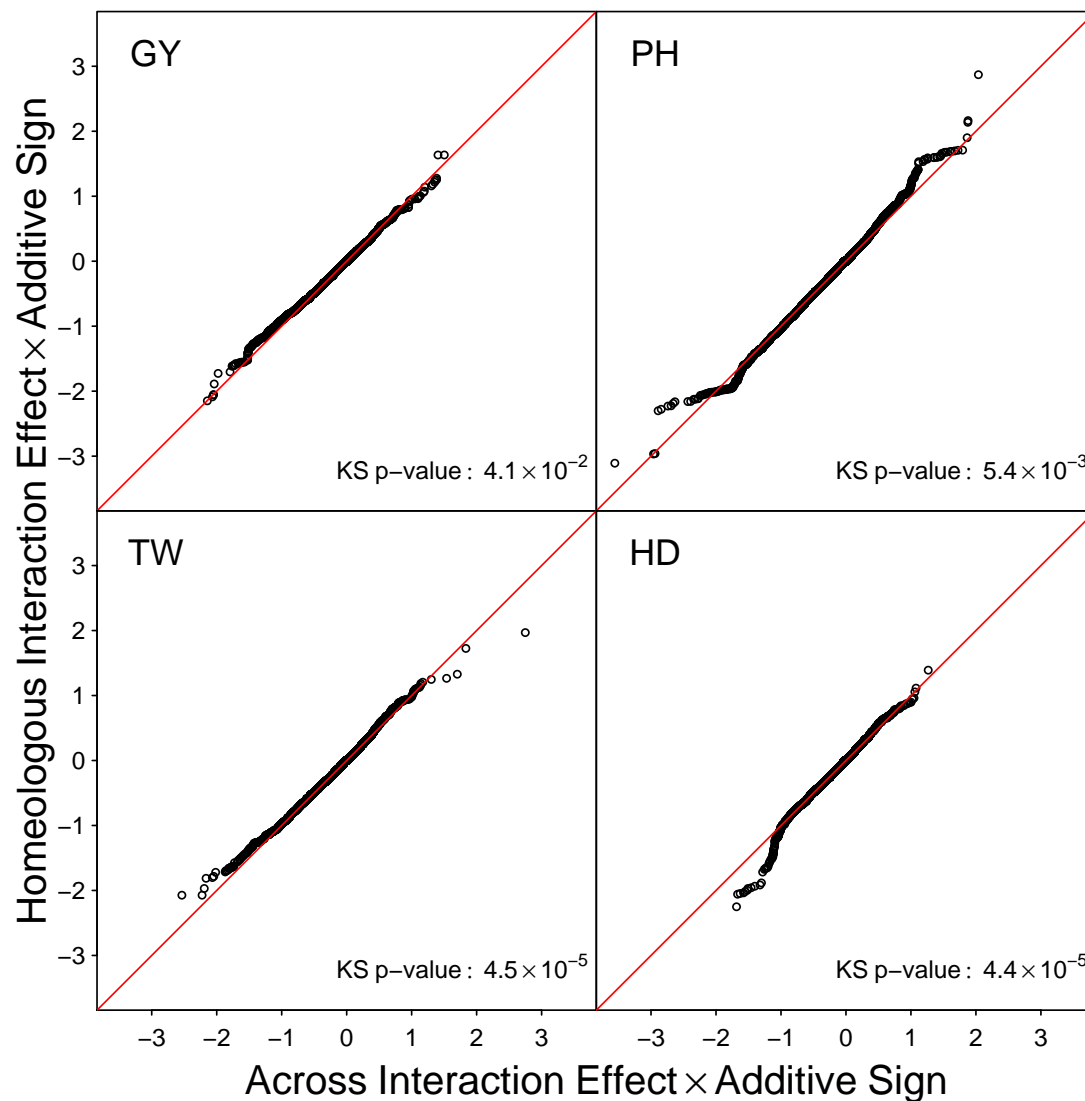
Figure S8: Quantile quantile plot of the ordered estimated homeologous interaction effects plotted against those from marker sets sampled across non-syntenic subgenome chromosomes (Across) using the LAVHAE marker orientation. Interaction effects have been multiplied by the effect sign of the corresponding additive effects to emphasize the relationship between the additive and interaction effects.
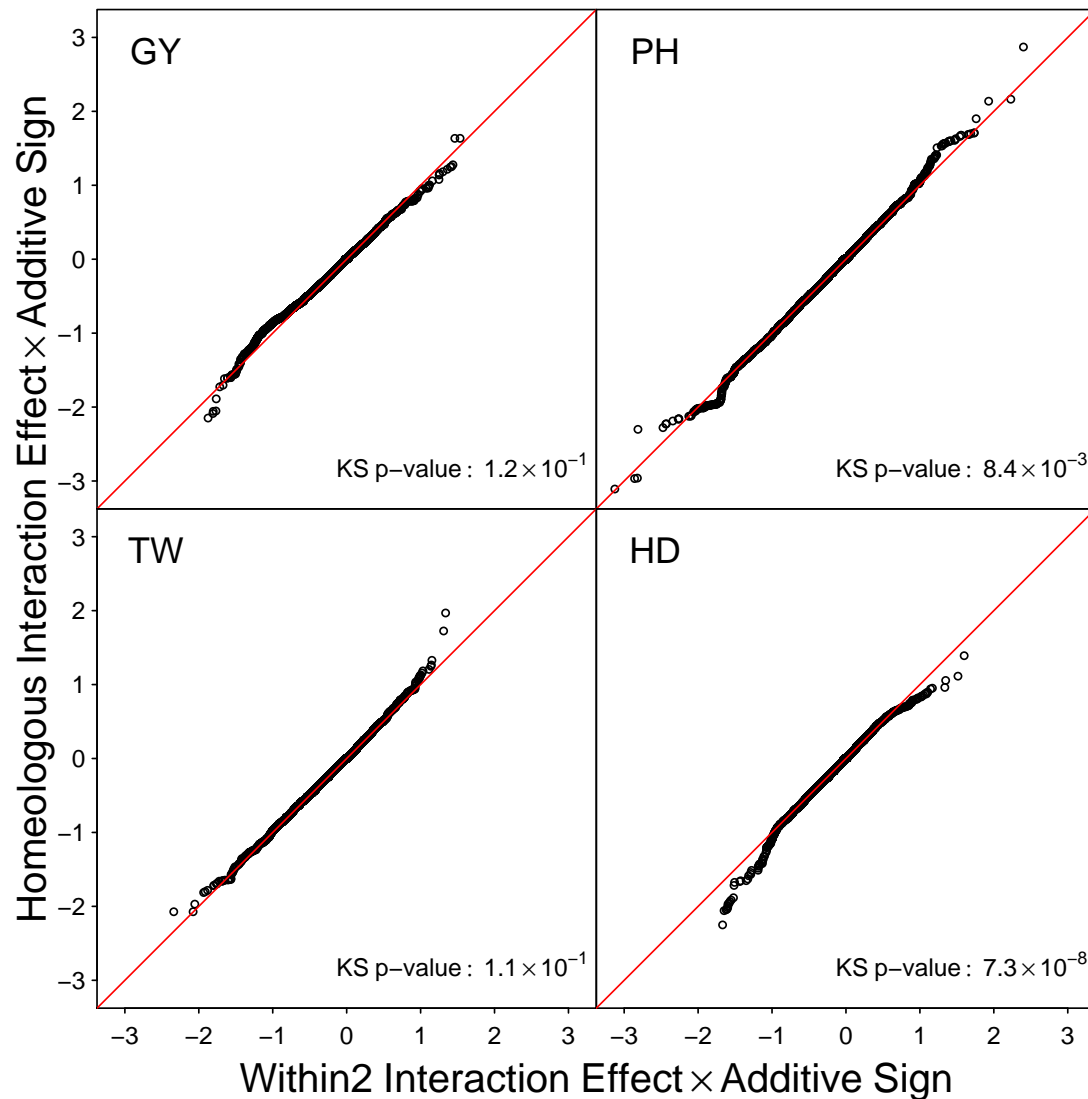
Figure S9: Quantile quantile plot of the ordered estimated homeologous interaction effects plotted against those from marker sets re-sampled within subgenome chromosomes (Within2) using the LAVHAE . Interaction effects have been multiplied by the effect sign of the corresponding additive effects to emphasize the relationship between the additive and interaction effects.
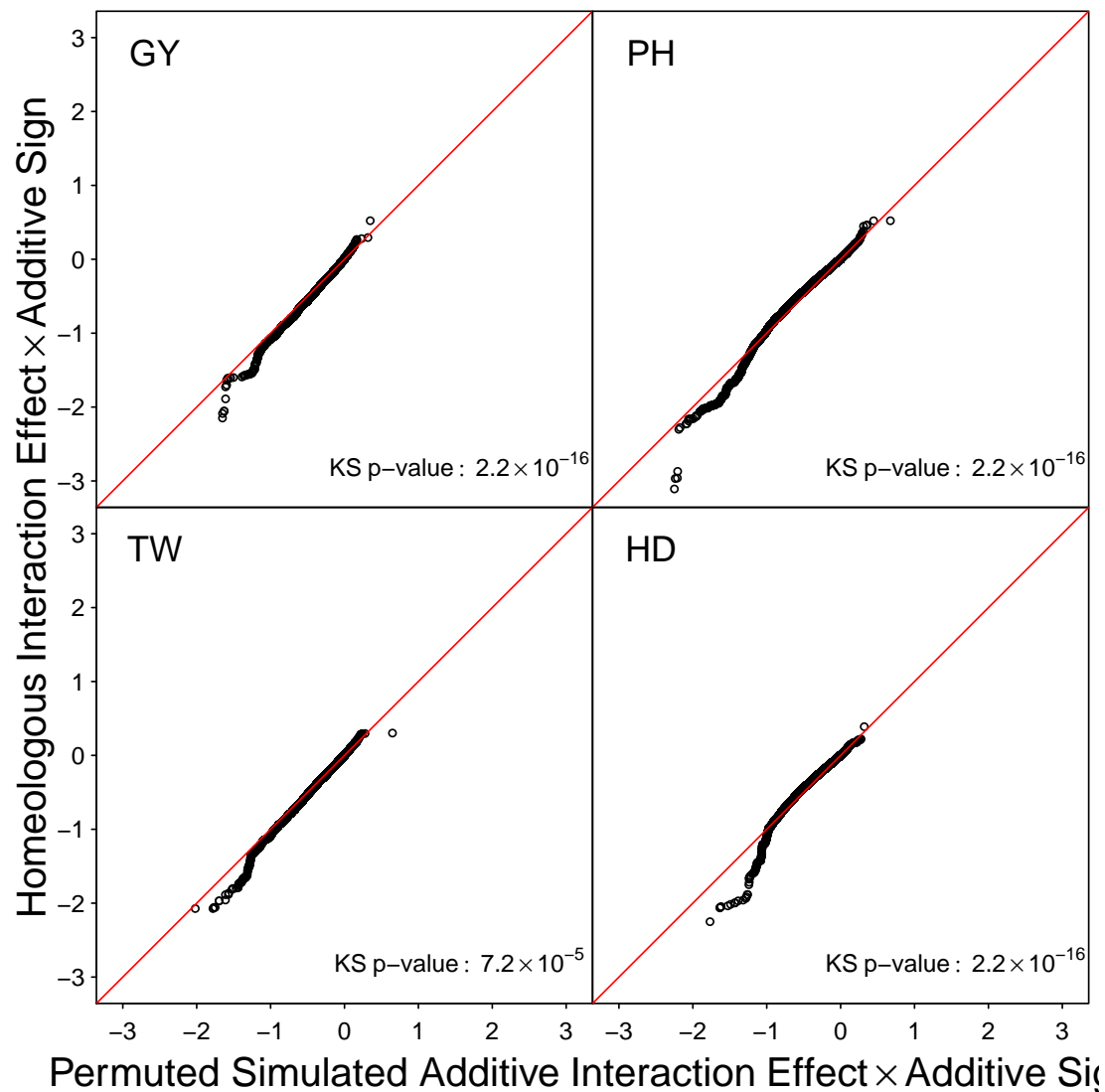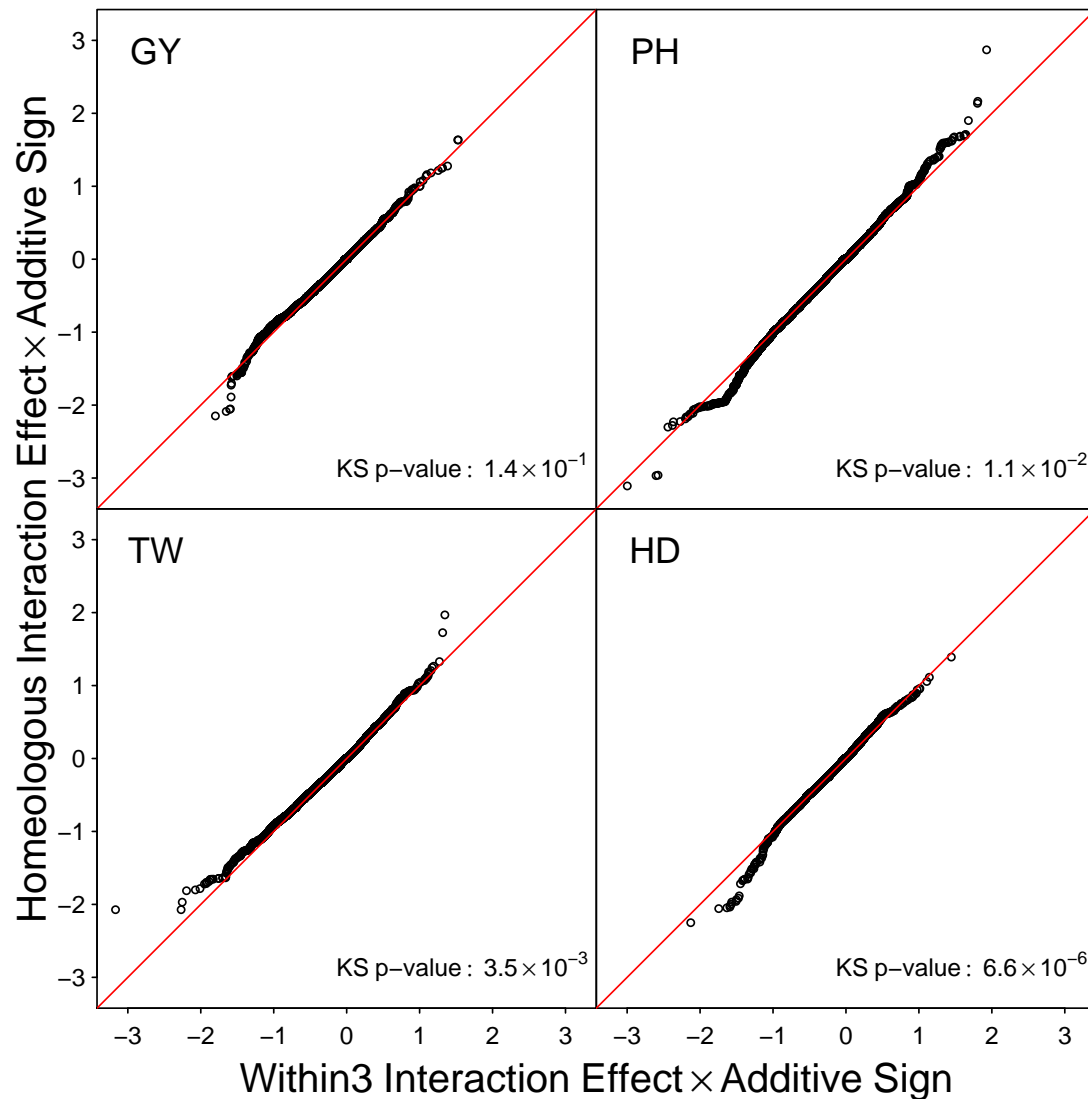
Figure S10: Quantile quantile plot of the ordered estimated homeologous interaction effects plotted against those from marker sets re-sampled within subgenome chromosomes (Within3) using the LAVHAE . Interaction effects have been multiplied by the effect sign of the corresponding additive effects to emphasize the relationship between the additive and interaction effects.
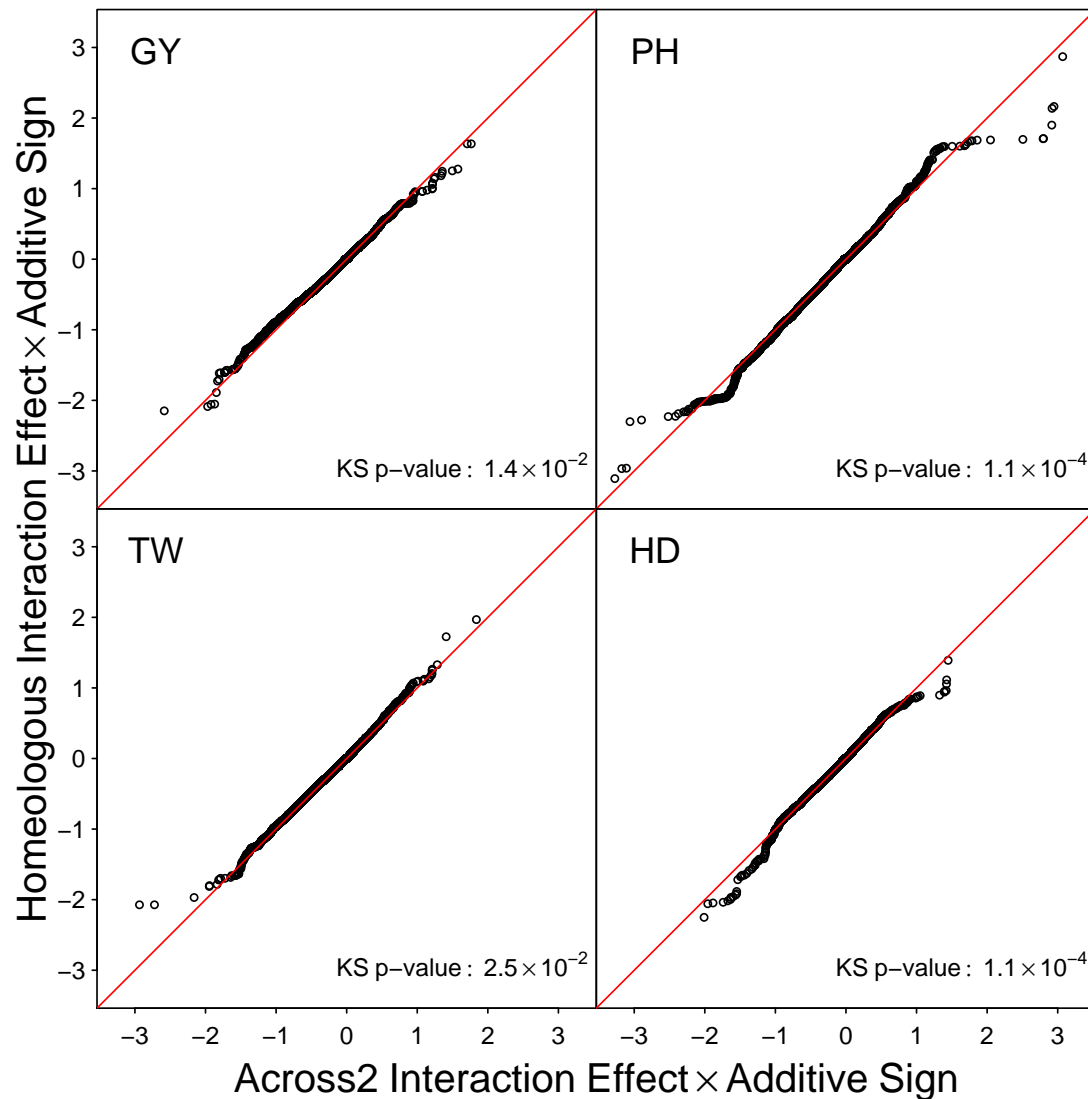
Figure S11: Quantile quantile plot of the ordered estimated homeologous interaction effects plotted against those from marker sets re-sampled across non-syntenic subgenome chromosomes (Across2) using the LAVHAE marker orientation. Interaction effects have been multiplied by the effect sign of the corresponding additive effects to emphasize the relationship between the additive and interaction effects.
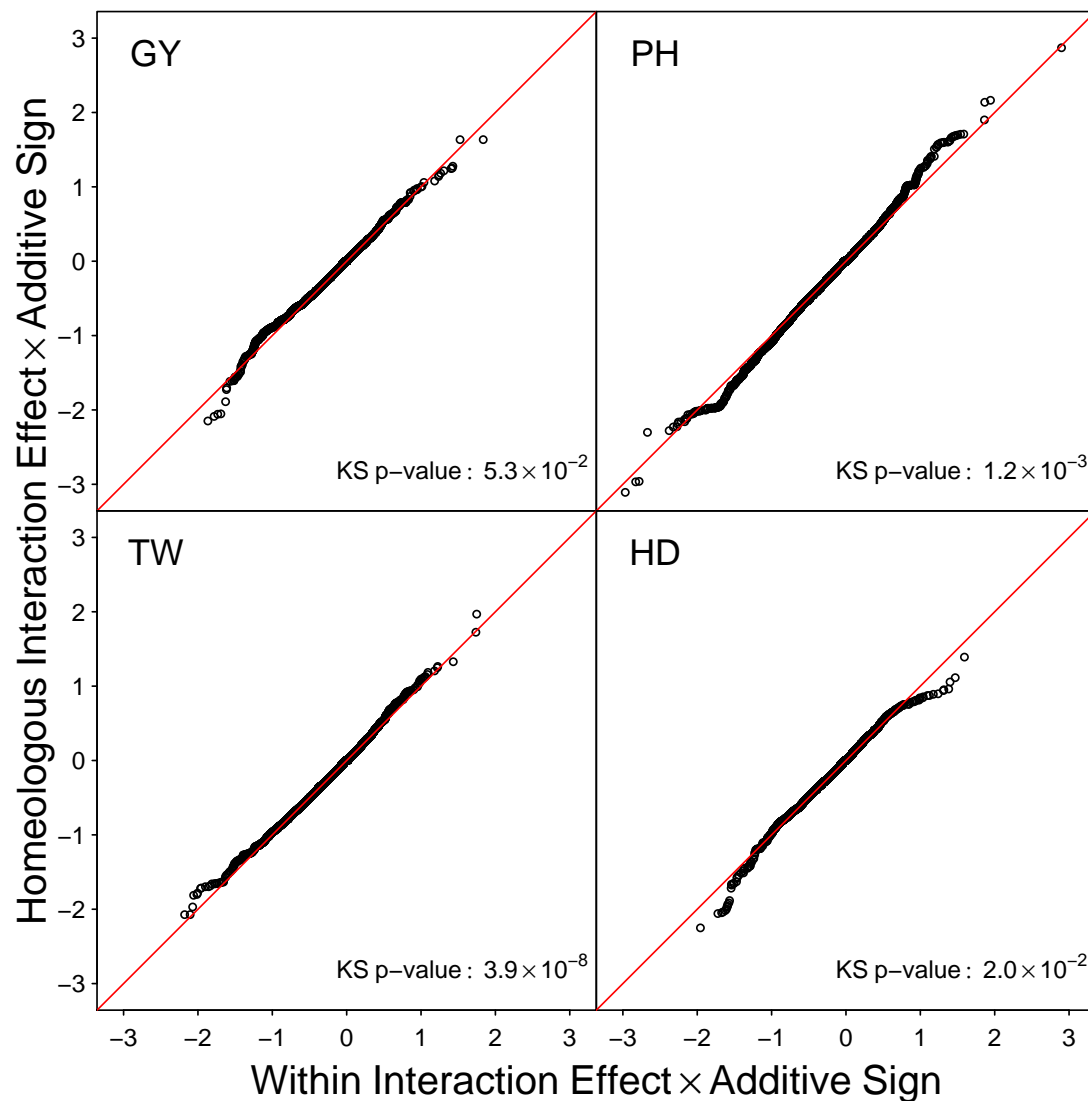
Figure S12: Quantile quantile plot of the ordered estimated homeologous interaction effects plotted against those from marker sets re-sampled across non-syntenic subgenome chromosomes (Across3) using the LAVHAE marker orientation. Interaction effects have been multiplied by the effect sign of the corresponding additive effects to emphasize the relationship between the additive and interaction effects.
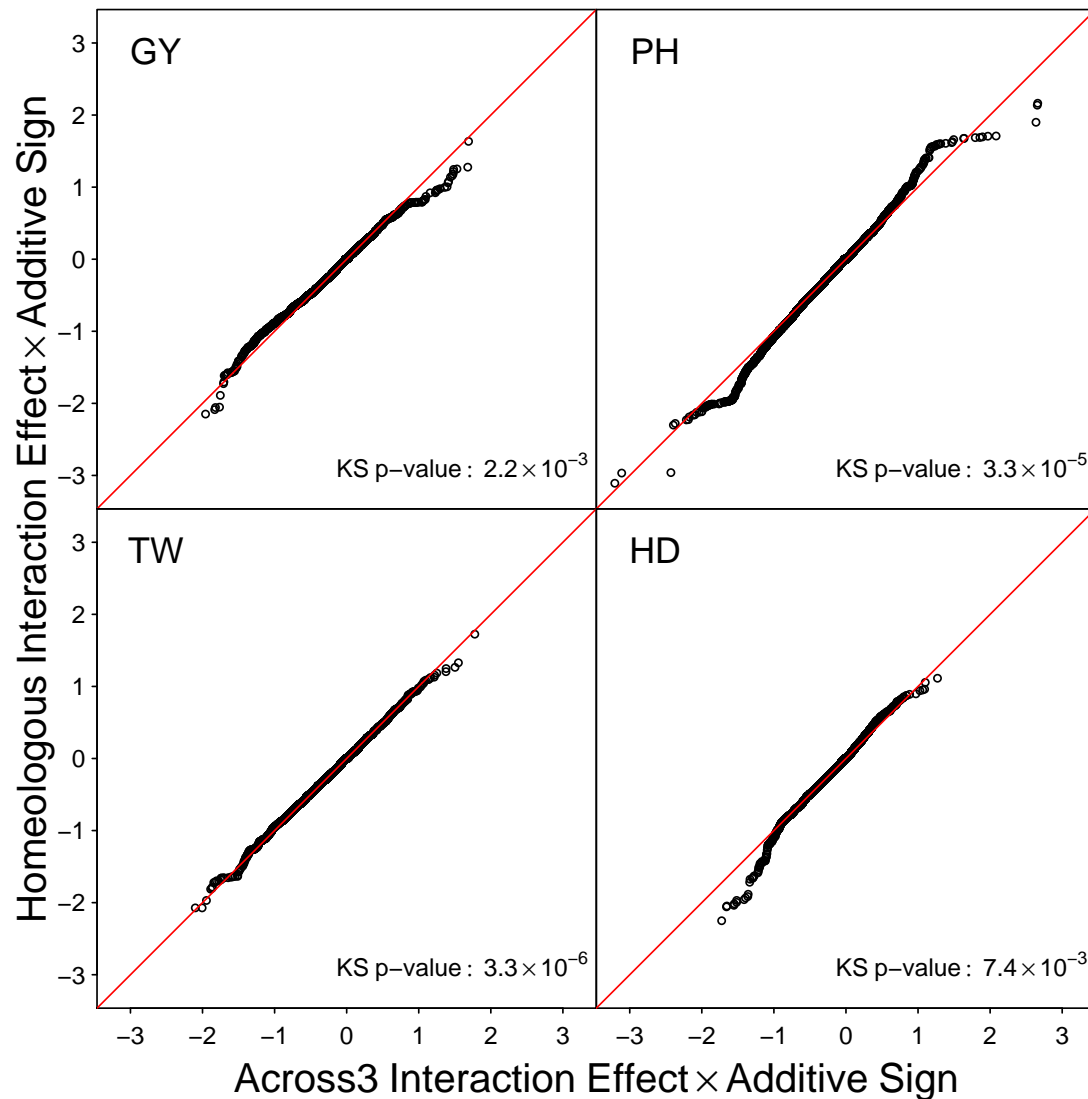
Table S4: Mixed model REML fit summaries of one additive and four epistasis models for four traits (GY, PH, TW and HD) in the CNLM population based on the $\{-1, 1\}$ marker parameterization using the LAVHAE marker orientation. Plot level heritabilities assuming genotype independence (i.i.d.) for each trait are shown underneath each trait name.

Trait		Additive	Pairwise	Homeo	Within	Across
GY	$\log\mathcal{L}$	-48	-43	-42	-26	-23
$h^2 = 0.30^a$	parameters	28	29	29	29	29
	AIC	153	144	141	110	104
	G	0.268^b $(12.59)^c$	0.203 (7.86)	0.204 (8.49)	0.133 (5.93)	0.13 (5.84)
	H		0.018 (3.04)	0.046 (3.29)^{***d}	0.093 (5.64)****	0.093 (5.77)****
	R	0.324 $(61.86)^e$	0.322 (61.39)	0.323 (61.68)	0.321 (61.7)	0.321 (61.7)
PH	$\log\mathcal{L}$	2237	2360	2314	2367	2374
$h^2 = 0.73$	parameters	26	27	27	27	27
	AIC	-4423	-4665	-4574	-4680	-4694
	G	3.823 (20.75)	0.889 (6.46)	1.882 (11.66)	0.986 (7.35)	1.046 (7.81)
	H		0.478 (11.95)	0.914 (8.72)****	1.277 (11.67)****	1.253 (11.62)****
	R	0.135 (56.17)	0.132 (56.5)	0.133 (56.34)	0.133 (56.45)	0.133 (56.5)
TW	$\log\mathcal{L}$	1547	1630	1608	1641	1632
$h^2 = 0.79$	parameters	28	29	29	29	29
	AIC	-3037	-3203	-3159	-3224	-3205
	G	1.067 (16.66)	0.194 (4.47)	0.442 (8.35)	0.212 (4.81)	0.221 (4.79)
	H		0.184 (11.33)	0.346 (8.39)****	0.473 (10.95)****	0.473 (10.66)****
	R	0.2 (60.12)	0.195 (60.25)	0.198 (60.24)	0.197 (60.35)	0.197 (60.31)
HD	$\log\mathcal{L}$	6343	6432	6404	6425	6444
$h^2 = 0.53$	parameters	27	28	28	28	28
	AIC	-12631	-12808	-12751	-12794	-12831
	G	3.9 (21.16)	1.121 (7.3)	2.019 (12.03)	1.483 (9.25)	1.212 (8.29)
	H		0.451 (11.13)	0.857 (8.26)****	1.091 (10.01)****	1.202 (10.97)****
	R	0.054 (58.76)	0.053 (58.98)	0.053 (58.88)	0.053 (58.93)	0.053 (58.96)

$^a h^2$ is the plot level trait heritability assuming genotype independence.

^{b}Variance component estimates reported for additive main effects (G) and epistatic interactions (H) are the ratios of the actual variance component to the residual variance component for ease of comparison.

^{c}The variance component divided by their respective standard errors are shown in parentheses.

^{d}*, **, ***, **** denote p-values of $p < 0.05$, $p < 0.01$, $p < 0.001$, $p < 10^{-6}$, respectively for the likelihood ratio test to determine if the epistatic variance component is zero.

^{e}The residual variance components, R, are the actual estimates from the centered and scaled data (refer to Santantonio *et al.* (2018b) for scaling coefficients).

Table S5: Mixed model REML fit summaries of three epistasis models for 4 traits (GY, PH, TW and HD) in the CNLM population based on the $\{0, 1\}$ marker parameterization using the LAVHAE marker orientation.

Trait		Homeo	Within	Across
GY	$\log\mathcal{L}$	-48	-47	-42
	parameters	29	29	29
	AIC	155	152	143
	G	0.267^a $(7.6)^b$	0.207 (5.5)	0.146 (4.16)
	H	0 (0.01)	0.054 (1.73)	0.108 $(3.39)^{***c}$
	R	0.324 $(61.81)^d$	0.324 (61.77)	0.324 (61.8)
PH	$\log\mathcal{L}$	2282	2268	2285
	parameters	27	27	27
	AIC	-4510	-4482	-4516
	G	1.198 (5.03)	1.766 (6.95)	1.177 (5.02)
	H	1.981 (8.36)****	1.592 (6.95)****	2.051 (8.66)****
	R	0.134 (56.23)	0.134 (56.24)	0.134 (56.24)
TW	$\log\mathcal{L}$	1560	1555	1567
	parameters	29	29	29
	AIC	-3061	-3052	-3076
	G	0.553 (5.88)	0.659 (6.68)	0.498 (5.57)
	H	0.414 (5.04)****	0.331 (4.06)***	0.482 (5.85)****
	R	0.199 (60.11)	0.199 (60.1)	0.198 (60.13)
HD	$\log\mathcal{L}$	6382	6364	6379
	parameters	28	28	28
	AIC	-12709	-12673	-12702
	G	1.51 (6.14)	2.077 (7.82)	1.659 (6.67)
	H	1.781 (7.73)****	1.358 (6.09)****	1.68 (7.36)****
	R	0.053 (58.84)	0.054 (58.78)	0.054 (58.81)

[a]Variance component estimates reported for additive main effects (G) and epistatic interactions (H) are the ratios of the actual variance component to the residual variance component for ease of comparison.

[b]The variance component divided by their respective standard errors are shown in parentheses.

[c]*, **, ***, **** denote p-values of $p < 0.05$, $p < 0.01$, $p < 0.001$, $p < 10^{-6}$, respectively for the likelihood ratio test to determine if the epistatic variance component is zero.

[d]The residual variance components, R, are the actual estimates from the centered and scaled data (refer to Santantonio *et al.* (2018b) for scaling coefficients).

Table S6: Mixed model REML fit summaries of three epistasis models for 4 traits (GY, PH, TW and HD) in the CNLM population based on the $\{-1, 1\}$ marker parameterization using the POS marker orientation.

Trait		Homeo	Within	Across
GY	$\log\mathcal{L}$	-48	-41	-40
	parameters	29	29	29
	AIC	154	140	138
	G	0.257^a $(10.31)^b$	0.191 (7.44)	0.186 (7.32)
	H	0.008 (0.75)	0.052 $(3.45)^{***c}$	0.054 (3.61)***
	R	0.324 $(61.7)^d$	0.323 (61.64)	0.323 (61.64)
PH	$\log\mathcal{L}$	2287	2323	2326
	parameters	27	27	27
	AIC	-4521	-4593	-4598
	G	2.316 (13.04)	1.507 (9.34)	1.551 (9.59)
	H	0.705 (7.3)****	1.056 (9.85)****	1.036 (9.72)****
	R	0.134 (56.29)	0.133 (56.38)	0.133 (56.4)
TW	$\log\mathcal{L}$	1589	1599	1604
	parameters	29	29	29
	AIC	-3120	-3139	-3150
	G	0.554 (9.49)	0.437 (7.44)	0.395 (7.02)
	H	0.282 (7.22)****	0.354 (8.36)****	0.368 (8.71)****
	R	0.198 (60.18)	0.197 (60.2)	0.197 (60.21)
HD	$\log\mathcal{L}$	6379	6393	6415
	parameters	28	28	28
	AIC	-12701	-12730	-12774
	G	2.547 (13.61)	2.017 (10.81)	1.689 (9.94)
	H	0.601 (6.43)****	0.848 (8.04)****	0.982 (9.26)****
	R	0.053 (58.83)	0.053 (58.87)	0.053 (58.92)

[a]Variance component estimates reported for additive main effects (G) and epistatic interactions (H) are the ratios of the actual variance component to the residual variance component for ease of comparison.

[b]The variance component divided by their respective standard errors are shown in parentheses.

[c]*, **, ***, **** denote p-values of $p < 0.05$, $p < 0.01$, $p < 0.001$, $p < 10^{-6}$, respectively for the likelihood ratio test to determine if the epistatic variance component is zero.

[d]The residual variance components, R, are the actual estimates from the centered and scaled data (refer to Santantonio *et al.* (2018b) for scaling coefficients).

Table S7: Mixed model REML fit summaries of three epistasis models for 4 traits (GY, PH, TW and HD) in the CNLM population based on the $\{-1, 1\}$ marker parameterization using the NEG marker orientation.

Trait		Homeo	Within	Across
GY	$\log\mathcal{L}$	-46	-38	-35
	parameters	29	29	29
	AIC	151	134	129
	G	0.236^a $(9.44)^b$	0.181 (7.35)	0.178 (7.35)
	H	0.022 (1.86)	0.058 $(3.9)^{***c}$	0.06 $(4.1)^{****}$
	R	0.324 $(61.71)^d$	0.323 (61.68)	0.322 (61.68)
PH	$\log\mathcal{L}$	2293	2336	2342
	parameters	27	27	27
	AIC	-4532	-4619	-4629
	G	2.235 (12.79)	1.428 (9.19)	1.464 (9.46)
	H	0.746 $(7.52)^{****}$	1.061 $(10.06)^{****}$	1.038 $(10.07)^{****}$
	R	0.134 (56.3)	0.133 (56.39)	0.133 (56.42)
TW	$\log\mathcal{L}$	1580	1605	1601
	parameters	29	29	29
	AIC	-3101	-3153	-3144
	G	0.614 (9.96)	0.373 (6.78)	0.388 (6.71)
	H	0.241 $(6.4)^{****}$	0.374 $(8.94)^{****}$	0.367 $(8.59)^{****}$
	R	0.199 (60.15)	0.198 (60.22)	0.197 (60.21)
HD	$\log\mathcal{L}$	6380	6402	6409
	parameters	28	28	28
	AIC	-12704	-12747	-12762
	G	2.48 (13.41)	1.88 (10.5)	1.753 (10.09)
	H	0.626 $(6.71)^{****}$	0.895 $(8.59)^{****}$	0.95 $(9.02)^{****}$
	R	0.053 (58.83)	0.053 (58.89)	0.053 (58.9)

[a]Variance component estimates reported for additive main effects (G) and epistatic interactions (H) are the ratios of the actual variance component to the residual variance component for ease of comparison.

[b]The variance component divided by their respective standard errors are shown in parentheses.

[c]*, **, ***, **** denote p-values of $p < 0.05$, $p < 0.01$, $p < 0.001$, $p < 10^{-6}$, respectively for the likelihood ratio test to determine if the epistatic variance component is zero.

[d]The residual variance components, R, are the actual estimates from the centered and scaled data (refer to Santantonio *et al.* (2018b) for scaling coefficients).

Table S8: Mixed model REML fit summaries of three epistasis models for 4 traits (GY, PH, TW and HD) in the CNLM population based on the $\{-1, 1\}$ marker parameterization using the HTEV marker orientation.

trait		Homeo	Within	Across
GY	$\log\mathcal{L}$	-46	-34	-30
	parameters	29	29	29
	AIC	151	127	118
	G	0.233^a $(9.23)^b$	0.165 (6.86)	0.151 (6.45)
	H	0.025 (1.97)	0.071 (4.56)****^{c}	0.079 (5)****
	R	0.323 $(61.65)^d$	0.322 (61.66)	0.322 (61.67)
PH	$\log\mathcal{L}$	2300	2355	2357
	parameters	27	27	27
	AIC	-4546	-4655	-4659
	G	2.052 (12.02)	1.101 (7.81)	1.142 (7.99)
	H	0.84 (8.12)****	1.227 (11.24)****	1.209 (11.09)****
	R	0.133 (56.32)	0.133 (56.43)	0.133 (56.46)
TW	$\log\mathcal{L}$	1599	1623	1623
	parameters	29	29	29
	AIC	-3140	-3189	-3187
	G	0.476 (8.51)	0.283 (5.73)	0.267 (5.4)
	H	0.335 (7.92)****	0.435 (10.13)****	0.45 (10.15)****
	R	0.198 (60.2)	0.197 (60.29)	0.197 (60.28)
HD	$\log\mathcal{L}$	6397	6410	6423
	parameters	28	28	28
	AIC	-12738	-12764	-12790
	G	2.13 (12.27)	1.62 (9.54)	1.395 (8.69)
	H	0.808 (7.9)****	1.029 (9.43)****	1.139 (10.18)****
	R	0.053 (58.88)	0.053 (58.91)	0.053 (58.94)

[a]Variance component estimates reported for additive main effects (G) and epistatic interactions (H) are the ratios of the actual variance component to the residual variance component for ease of comparison.

[b]The variance component divided by their respective standard errors are shown in parentheses.

[c]*, **, ***, **** denote p-values of $p < 0.05$, $p < 0.01$, $p < 0.001$, $p < 10^{-6}$, respectively for the likelihood ratio test to determine if the epistatic variance component is zero.

[d]The residual variance components, R, are the actual estimates from the centered and scaled data (refer to Santantonio *et al.* (2018b) for scaling coefficients).

Table S9: Mixed model REML fit summaries of three epistasis models for 4 traits (GY, PH, TW and HD) in the CNLM population based on the $\{0, 1\}$ marker parameterization using the HTEV marker orientation.

trait		Homeo	Within	Across
GY	$\log\mathcal{L}$	-48	-48	-48
	parameters	29	29	29
	AIC	155	155	155
	G	0.268^a $(12.59)^b$	0.268 (12.59)	0.268 (12.59)
	H	0	0	0
	R	0.324 $(61.86)^c$	0.324 (61.86)	0.324 (61.86)
PH	$\log\mathcal{L}$	2260	2246	2248
	parameters	27	27	27
	AIC	-4466	-4438	-4443
	G	1.981 (7.41)	2.84 (9.98)	2.502 (8.49)
	H	1.423 $(6.05)^{****d}$	0.806 (3.68)***	1.081 (4.44)***
	R	0.134 (56.2)	0.134 (56.19)	0.134 (56.19)
TW	$\log\mathcal{L}$	1552	1547	1549
	parameters	29	29	29
	AIC	-3046	-3036	-3041
	G	0.746 (7.61)	0.992 (9.51)	0.857 (8.24)
	H	0.264 (3.38)***	0.064 (0.87)	0.183 (2.26)*
	R	0.199 (60.1)	0.199 (60.08)	0.199 (60.09)
HD	$\log\mathcal{L}$	6358	6350	6356
	parameters	28	28	28
	AIC	-12660	-12643	-12656
	G	2.528 (9.24)	2.937 (10.1)	2.468 (8.5)
	H	1.052 (4.83)****	0.749 (3.44)***	1.16 (4.78)****
	R	0.054 (58.79)	0.054 (58.76)	0.054 (58.78)

[a]Variance component estimates reported for additive main effects (G) and epistatic interactions (H) are the ratios of the actual variance component to the residual variance component for ease of comparison.

[b]The variance component divided by their respective standard errors are shown in parentheses.

[c]The residual variance components, R, are the actual estimates from the centered and scaled data (refer to Santantonio *et al.* (2018b) for scaling coefficients).

[d]*, **, ***, **** denote p-values of $p < 0.05$, $p < 0.01$, $p < 0.001$, $p < 10^{-6}$, respectively for the likelihood ratio test to determine if the epistatic variance component is zero.

Table S10: Mixed model REML fit summaries of four epistasis models for 4 traits (GY, PH, TW and HD) in the CNLM population based on the $\{-1, 1\}$ marker parameterization using the LAVHAE marker orientation using two additional samples of Within (Within2, Within3) and Across (Across2, Across3).

Trait		Within2	Within3	Across2	Across3
GY	$\log\mathcal{L}$	-32	-29	-26	-32
	parameters	29	29	29	29
	AIC	122	115	110	121
	G	0.15^a $(6.29)^b$	0.14 (6.07)	0.134 (5.91)	0.154 (6.55)
	H	0.081 $(4.97)^{****c}$	0.086 $(5.32)^{****}$	0.092 $(5.58)^{****}$	0.078 $(4.89)^{****}$
	R	0.322 $(61.67)^d$	0.322 (61.7)	0.321 (61.69)	0.322 (61.67)
PH	$\log\mathcal{L}$	2369	2356	2357	2359
	parameters	27	27	27	27
	AIC	-4685	-4658	-4661	-4664
	G	0.979 (7.38)	1.066 (7.57)	1.083 (7.67)	1.103 (7.86)
	H	1.257 $(11.59)^{****}$	1.242 $(11.23)^{****}$	1.253 $(11.27)^{****}$	1.23 $(11.27)^{****}$
	R	0.133 (56.45)	0.133 (56.44)	0.133 (56.44)	0.133 (56.48)
TW	$\log\mathcal{L}$	1647	1627	1641	1634
	parameters	29	29	29	29
	AIC	-3235	-3196	-3224	-3210
	G	0.2 (4.56)	0.267 (5.42)	0.213 (4.74)	0.233 (5)
	H	0.479 $(10.94)^{****}$	0.441 $(10.11)^{****}$	0.48 $(10.86)^{****}$	0.472 $(10.67)^{****}$
	R	0.197 (60.38)	0.197 (60.29)	0.196 (60.31)	0.196 (60.36)
HD	$\log\mathcal{L}$	6455	6429	6442	6444
	parameters	28	28	28	28
	AIC	-12853	-12801	-12828	-12832
	G	1.053 (7.75)	1.366 (8.76)	1.174 (8.15)	1.173 (8.15)
	H	1.311 $(11.68)^{****}$	1.15 $(10.39)^{****}$	1.248 $(11.19)^{****}$	1.226 $(11.11)^{****}$
	R	0.053 (58.99)	0.053 (58.94)	0.053 (58.94)	0.053 (58.95)

[a] Variance component estimates reported for additive main effects (G) and epistatic interactions (H) are the ratios of the actual variance component to the residual variance component for ease of comparison.

[b] The variance component divided by their respective standard errors are shown in parentheses.

[c] *, **, ***, **** denote p-values of $p < 0.05$, $p < 0.01$, $p < 0.001$, $p < 10^{-6}$, respectively for the likelihood ratio test to determine if the epistatic variance component is zero.

[d] The residual variance components, R, are the actual estimates from the centered and scaled data (refer to Santantonio *et al.* (2018b) for scaling coefficients).

Table S11: Mixed model REML fit summaries of four epistasis models for 4 traits (GY, PH, TW and HD) in the CNLM population based on the $\{0, 1\}$ marker parameterization using the LAVHAE marker orientation using two additional samples of within and across markers.

Trait		Within2	Within3	Across2	Across3
GY	log$\mathcal{L}$	-47	-48	-48	-48
	parameters	29	29	29	29
	AIC	153	155	154	154
	G	0.213^a $(5.66)^b$	0.25 (6.62)	0.235 (6.47)	0.248 (6.74)
	H	0.048 (1.56)	0.015 (0.53)	0.03 (1.06)	0.017 (0.62)
	R	0.324 $(61.78)^c$	0.324 (61.79)	0.324 (61.75)	0.324 (61.78)
PH	log$\mathcal{L}$	2268	2273	2265	2271
	parameters	27	27	27	27
	AIC	-4482	-4491	-4476	-4487
	G	1.867 (7.5)	1.656 (6.6)	1.929 (7.38)	1.742 (6.87)
	H	1.439 $(6.69)^{****\,d}$	1.682 (7.26)****	1.487 (6.49)****	1.623 (7.04)****
	R	0.134 (56.21)	0.134 (56.24)	0.134 (56.25)	0.134 (56.24)
TW	log$\mathcal{L}$	1564	1562	1557	1559
	parameters	29	29	29	29
	AIC	-3070	-3067	-3057	-3059
	G	0.49 (5.23)	0.53 (5.62)	0.657 (6.85)	0.589 (6.09)
	H	0.492 (5.67)****	0.464 (5.39)****	0.348 (4.31)***	0.401 (4.76)***
	R	0.198 (60.13)	0.198 (60.11)	0.199 (60.1)	0.199 (60.11)
HD	log$\mathcal{L}$	6381	6363	6371	6370
	parameters	28	28	28	28
	AIC	-12706	-12669	-12686	-12684
	G	1.364 (5.48)	2.291 (8.48)	1.63 (6.2)	1.994 (7.78)
	H	1.932 (8.04)****	1.194 (5.46)****	1.756 (7.18)****	1.406 (6.42)****
	R	0.054 (58.81)	0.054 (58.78)	0.054 (58.8)	0.054 (58.78)

[a]Variance component estimates reported for additive main effects (G) and epistatic interactions (H) are the ratios of the actual variance component to the residual variance component for ease of comparison.

[b]The variance component divided by their respective standard errors are shown in parentheses.

[c]The residual variance components, R, are the actual estimates from the centered and scaled data (refer to Santantonio *et al.* (2018b) for scaling coefficients).

[d]*, **, ***, **** denote p-values of $p < 0.05$, $p < 0.01$, $p < 0.001$, $p < 10^{-6}$, respectively for the likelihood ratio test to determine if the epistatic variance component is zero.

Table S12: Prediction accuracies of Homeo, Within and Across genome marker sets for both $\{-1, 1\}$ and $\{0, 1\}$ marker coding using POS marker orientation.

POS	Homeo_{-11}	Homeo_{01}	Within_{-11}	Within_{01}	Across_{-11}	Across_{01}
GY	0.599^a	0.599	0.607	0.600	0.607	0.599
PH	0.583	0.573	0.607	0.568	0.612	0.576
TW	0.535	0.518	0.543	0.514	0.547	0.524
HD	0.681	0.681	0.688	0.670	0.698	0.671

^{a}Mean Pearson correlation between predicted and observed genetic values across 10 random 5-fold cross-validation replications.

Table S13: Prediction accuracies of Homeo, Within and Across genome marker sets for both $\{-1, 1\}$ and $\{0, 1\}$ marker coding using NEG marker orientation.

NEG	Homeo_{-11}	Homeo_{01}	Within_{-11}	Within_{01}	Across_{-11}	Across_{01}
GY	0.602^a	0.599	0.612	0.599	0.615	0.600
PH	0.589	0.582	0.620	0.565	0.615	0.579
TW	0.535	0.513	0.555	0.510	0.546	0.519
HD	0.676	0.671	0.698	0.671	0.697	0.680

^{a}Mean Pearson correlation between predicted and observed genetic values across 10 random 5-fold cross-validation replications.

Table S14: Prediction accuracies of Homeo, Within and Across genome marker sets for both $\{-1, 1\}$ and $\{0, 1\}$ marker coding using HTEV marker orientation.

HTEV	Homeo_{-11}	Homeo_{01}	Within_{-11}	Within_{01}	Across_{-11}	Across_{01}
GY	0.601^a	0.601	0.616	0.600	0.621	0.600
PH	0.591	0.565	0.640	0.557	0.633	0.558
TW	0.548	0.513	0.572	0.513	0.568	0.513
HD	0.688	0.669	0.700	0.666	0.706	0.667

^{a}Mean Pearson correlation between predicted and observed genetic values across 10 random 5-fold cross-validation replications.

Table S15: Prediction accuracies of two additional samples of Within (Within2, Within3) and Across (Across2, Across3) genome marker sets, for both $\{-1, 1\}$ and $\{0, 1\}$ marker coding using LAVHAE marker orientation.

LAVHAE	Within2$_{01}$	Within3$_{01}$	Across2$_{01}$	Across3$_{01}$	Within2$_{-11}$	Within3$_{-11}$	Across2$_{-11}$	Across3$_{-11}$
GY	0.600	0.599	0.600	0.600	0.620	0.624	0.623	0.618
PH	0.573	0.569	0.566	0.570	0.655	0.640	0.634	0.644
TW	0.522	0.524	0.518	0.518	0.604	0.581	0.592	0.585
HD	0.683	0.673	0.676	0.679	0.727	0.715	0.718	0.724

71

Table S16: Estimates of s coefficients for marker sets where both additive and the two-way interaction effects were significant at $p < 0.05$ for each of 4 traits. The expected number of non-zero additive and two-way interactions effects based on a 0.05 significance threshold by chance for each trait is 3 (i.e. 22,411 two-way interactions $\times$ 0.05^3). Coefficients have been grouped by categories related to the potential mode of epistasis, where $s < 0.5$ indicates a highly negative interaction, $0.5 \leq s < 1$ a less-than-additive interaction may be indicative of subfunctionalization for homeologous genes, and $s > 1$ which indicates positive, or greater-than-additive, epistasis. Three marker sets are shown, either across all homeologous loci (Homeo), sampled sets within (Within) and across (Across) non-syntenic subgenome regions. An additional phenotype was simulated to contain additive only phenotypes to contain no epistasis, and fit with the Homeo marker set (Simulated Additive).

Marker Set	Trait	$s < 0.5$	$0.5 \leq s < 1$	$s > 1$	Total[a]
Homeo	GY	0	0	2	2
Homeo	PH	2	8	4	14***
Homeo	TW	5	4	2	11**
Homeo	HD	1	2	0	3
Simulated Additive	PH	0	1	3	4
Simulated Additive	HD	1	0	1	2
Across	GY	2	2	1	5
Across	PH	3	0	0	3
Across	TW	2	1	0	3
Across	HD	2	4	0	6*
Within	GY	1	1	0	2
Within	PH	2	1	3	6*
Within	TW	1	1	1	3
Within	HD	2	0	0	2

[a]*, **, *** indicate significantly greater than the expected number of significant sets at p = 0.05, 10^{-4} and 10^{-6} based the binomial distribution with 22,411 trials and a probability of 0.05^3.
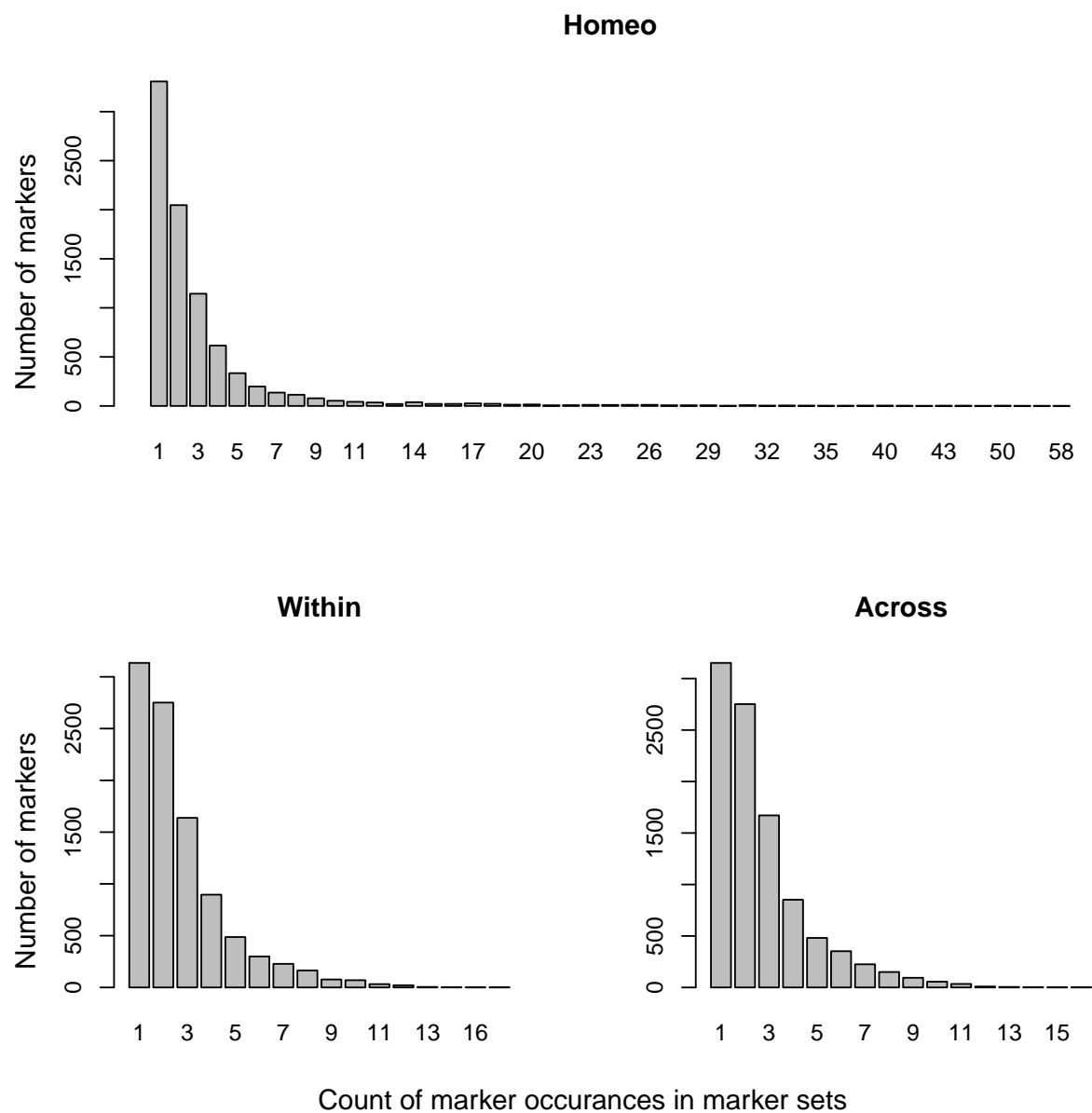
Figure S13: Distribution of the number of marker occurrences in marker sets. An occurrence of 1 indicates that a marker was only included in one marker set, whereas an occurrence of 10 would indicate that the marker was included in 10 marker sets.
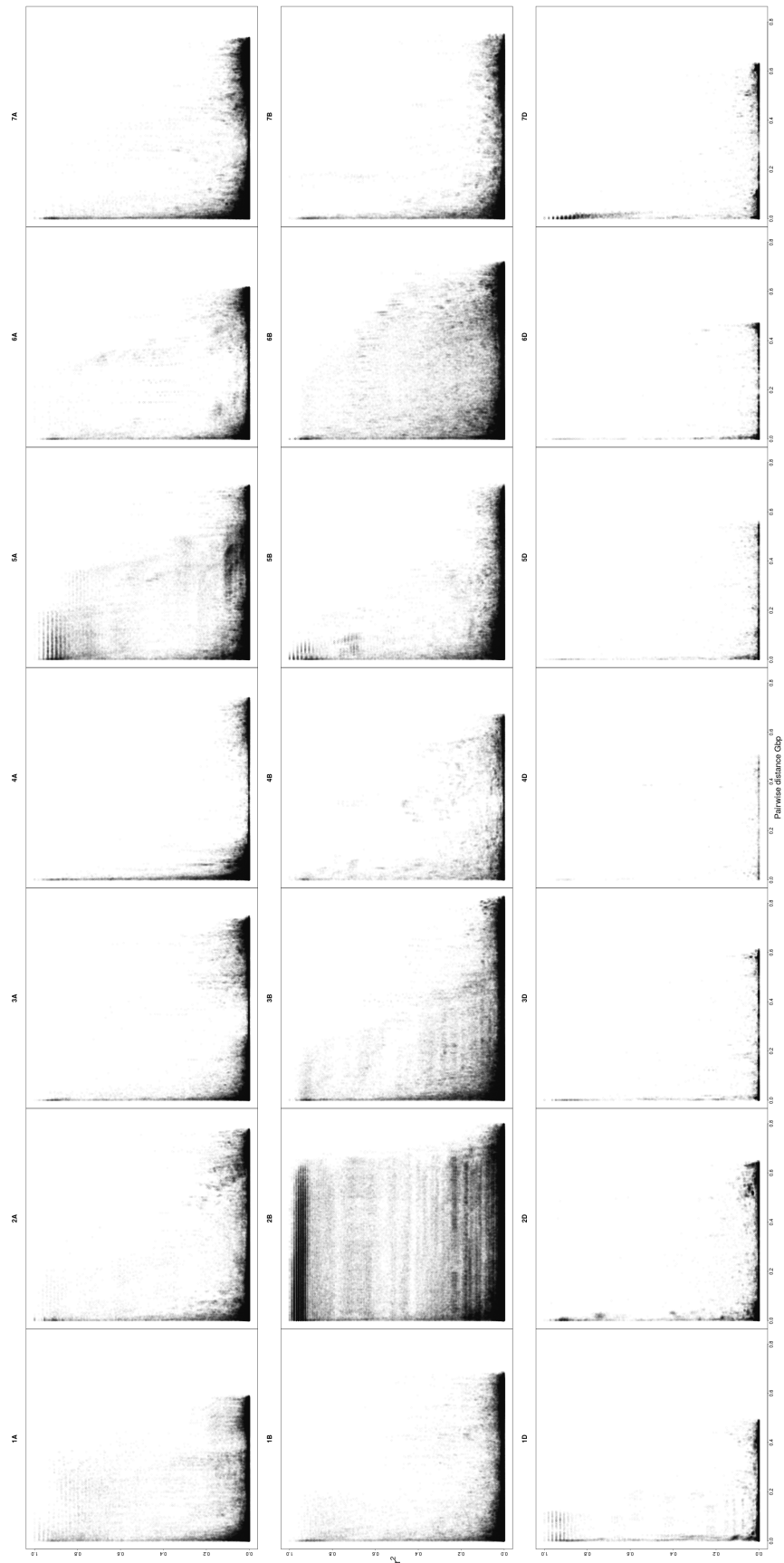
Figure S14: Pairwise linkage disequilibrium r^2 values for the 21 wheat chromosomes in the CNLM population.

74